DEPARTMENT OF PHYSICS, IIT BOMBAY

B.Tech Project

PH587

The Solar Abundance Problem: Gravitational Helioseismology

Manan Seth
190260028
BTech, Engineering Physics

Mentor:
Prof. Vikram Rentala
Department of Physics

April 26, 2023

Contents

1 Acknowledgements

Particle physics and astrophysics have fascinated me for quite a long time, and I would like to thank Prof. Vikram Rentala for giving me the opportunity to explore these fields through the Solar Abundance Problem. I am grateful for his guidance and advice, that introduced me to the world of research.

I would also like to thank Siddhant Tripathy, B. Malavika, Aman Avasthi and Eleena Gupta, my team members for this project who have mentored me from the start and helped me out whenever I have been facing issues with patience and enthusiasm.

2 Introduction

The Sun has been a natural observatory for scientific experiments for millennia. Not only does it provide a glimpse into the outside universe, it also acts as an excellent observatory for testing our theories of particle physics, by being able to produce particles of energies much higher than those possible with our best particle accelerators. It has been rigorously studied to constrain the properties of dark matter, and continues to provide new paths to study these elusive particles.

New revisions to the solar abundances have put two independent theories of the Sun at conflict - paving way for new physics. The metallicity of stars play a massive role in their evolution, affecting parameters such as opacity profiles, nuclear reaction rates, temperature gradients etc. The new data provides a lower metallicity value, which shifts the sound speed profile in standard solar models. However, this shifted value does not match the observed sound speed profile obtained by helioseismic inversions. Some other parameters affected by the lower metallicity are surface helium abundance, radius of the tachoclyne and the density profile.

This report will first cover some of the necessary background for this work, starting from major equations of stellar structure. We will then study the dynamic model of solar oscillations and their implications. After these 'prerequisites', we will look at a model of the sun that involves an additional non-diffusive transfer of energy in the solar radiation zone to fix the discrepencies between the models, and then a physical model involving millicharged particles to explain such a transfer of energy. Finally, we will study the possibility of probing g-modes through gravitational wave observations, and the feasability of detection by the upcoming space based detector LISA by using the current observational limits and computational modelling.

3 Modelling the Stellar Structure

3.1 Equations of Stellar Structure

We begin by trying to model the sun by stating some simplifying assumptions leading to some equations, stated without proof.

1. **Spherical Symmetry:** Assuming spherical symmetry allows us to treat various quantities as one-dimensional functions of radius and greatly simplifies calculations
2. **Mass Conservation:** We assume that the rate of mass lost by the sun is negligible compared to the total solar mass, $M_\odot$, over large time frames. This leads to the following equation
$$\frac{dM_r}{dr} = 4\pi r^2 \rho \tag{3.1}$$
where ρ is the density at r.
3. **Hydrostatic Equilibrium:** This comes from the long term stability of the sun in the form
$$\frac{dP}{dr} = -\frac{GM_r\rho}{r^2} \tag{3.2}$$
4. **Energy Conservation:** The energy emitted as part of the solar luminosity L must be generated by energy sources within
$$\frac{dL_r}{dr} = 4\pi r^2 \rho(\epsilon + \epsilon_{gr} - \epsilon_\nu) \tag{3.3}$$
Here L_r is the luminosity at r flowing through an infinitesimal shell, ϵ is the energy generated per unit mass per second by nuclear fusion processes, ϵ_{gr} is the energy absorbed or released due to gravitational expansions or contractions, and ϵ_ν is the energy lost to neutrino emission.
5. **Energy Transport:** The temperature gradient in the sun is a handy way to quantify the rate of energy transport in the following equation
$$\frac{dT}{dr} = -\frac{GM_rT}{r^2P}\nabla = -\frac{GM_rT}{r^2P}\frac{d\ln T}{d\ln P} \tag{3.4}$$
Where ∇ is the dimensionless 'temperature gradient'. This depends on the nature of energy transport - convective or radiative being the dominant modes in the sun.
6. **Schwarzschild Criterion for Convection:** As mentioned, ∇ depends on the mode of energy transport. For radiative energy transport, we have
$$\nabla = \nabla_{rad} = \frac{3}{64\pi\sigma G}\frac{\kappa L_r P}{M_r T^4} \tag{3.5}$$
Here σ is the Stefan-Boltzman constant, κ is the opacity function and T is the temperature as a function of r.

For convective energy transport, in adiabatic conditions, we have,

$$\nabla_{ad} \equiv (\partial \ln T / \partial \ln P)_s \tag{3.6}$$

where s is the specific entropy.

Finally, the Schwarzschild Criterion states that we will have convection when

$$\nabla_{\text{rad}} > \nabla_{\text{ad}} \tag{3.7}$$

7. **Chemical Composition:** Chemical compositions of elements as a function of radius can change with time due to factors such as

   - Nuclear reactions affecting abundance of a particular isotope:

   $$\frac{\partial X_i}{\partial t} = \frac{m_i}{\rho}\left[\sum_j r_{ji} - \sum_k r_{ik}\right] \tag{3.8}$$

   where X_i is the mass fraction of the isotope in consideration, m_i the respective mass, r_{ji} is the rate of production from element j, and r_{ik} is the rate of conversion to another element or isotope k.

   - Diffusion and gravitational settling, given by

   $$\frac{\partial X_i}{\partial t} = D\nabla^2 X_i \tag{3.9}$$

   where D is the diffusion parameter

   - The rate at which the average abundance of any species i in the convection zone changes will depend on nuclear reactions in the convection zone, as well as the mass limits of spherical shells of radiative and convective zones.

3.2 Mixing Length Theory

The mixing length theory models energy transport through macroscopic eddies, whose mean free path can be modelled in terms of the mixing length parameter α_{MLT} as

$$l_m = \alpha_{MLT} H_P \tag{3.10}$$

where $H_P = -dr/d(\ln P)$ is the pressure scale height.

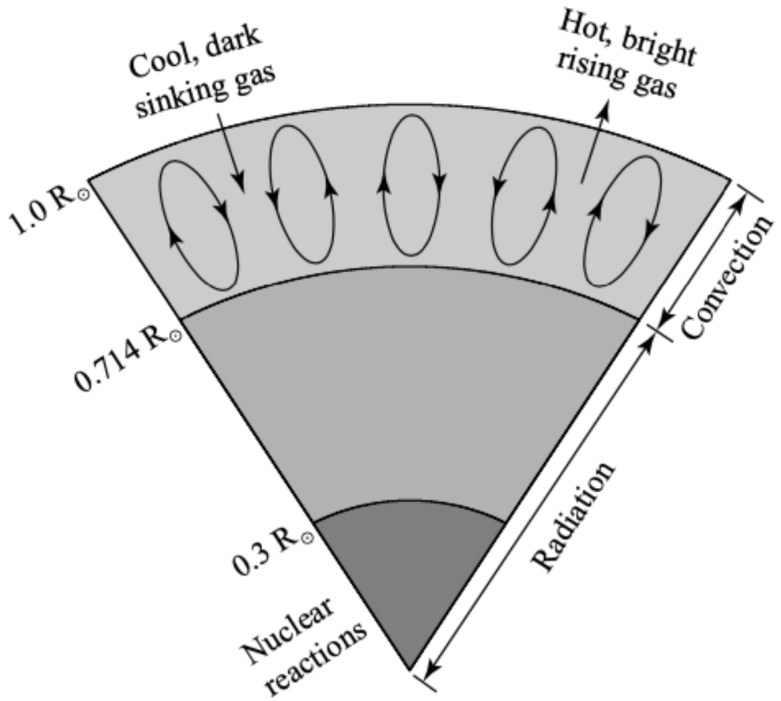

Figure 1: Major layers in the standard solar model (Carroll & Ostlie, 2017)

3.3 The Standard Solar Model (SSM)

Until now, we have five unknowns (M_r, ρ, P, L_r and T) and four equations. Thus, we need another equation of state which models the atomic interactions, ionization rates and so on (Basu & Antia, 2008). Popular models of the equation of state are OPAL, MHD and CEFF. This completes our solar model once we provide the following additional parameters:

- **Opacity function** κ: These are generated by modelling inter-particle interactions at various temperatures and densities, and interpolating the singular data points. The OPAL tables are a popular choice for simulated data.
- **Nuclear reaction rates:** We need to provide the nuclear reaction rates, composition changes and neutrino fluxes from a mixture of laboratory measurements and theoretical calculations.
- **Boundary Conditions:** (Carroll & Ostlie, 2017)
  as $r \longrightarrow 0 : M_r, L_r \longrightarrow 0$
  as $r \longrightarrow R_* : T, P, \rho \longrightarrow 0$, where R_* is the star's radius.

Standard Solar Models (SSMs) (Bergemann & Serenelli, 2014) are 1D models for a $1\,M_\odot$ star, starting from a homogeneous model in the pre-main sequence up to the present-day age of the solar system, i.e. $\tau_\odot = 4.57$Gyr. These must follow the following constraints:

- Present-day luminosity $L_\odot = 3.8418 \times 10^{33}$ ers s^{-1}
- Radius $R_\odot = 6.9598 \times 10^{10}$ cm

- $(Z/X)_\odot$, Z is the metallic abundance and X is hydrogen abundance of the Sun.

The following parameters can be tuned to satisfy the above observational constraints:

- The mixing length parameter α_{MLT}
- Initial helium mass fraction Y_{ini}
- Initial metallicity X_{ini}

Of course we also have a third constraint $X + Y + Z = 1$, where X is the hydrogen mass fraction.

For every model, there are different sources from which $(Z/X)_\odot$ are identified, different equations of state and so on. Thus, different groups have have different standard solar models, and assumptions for each must be carefully studied.

We are now able to model the variables in the solar interior and obtain the following results for a type of SSM:

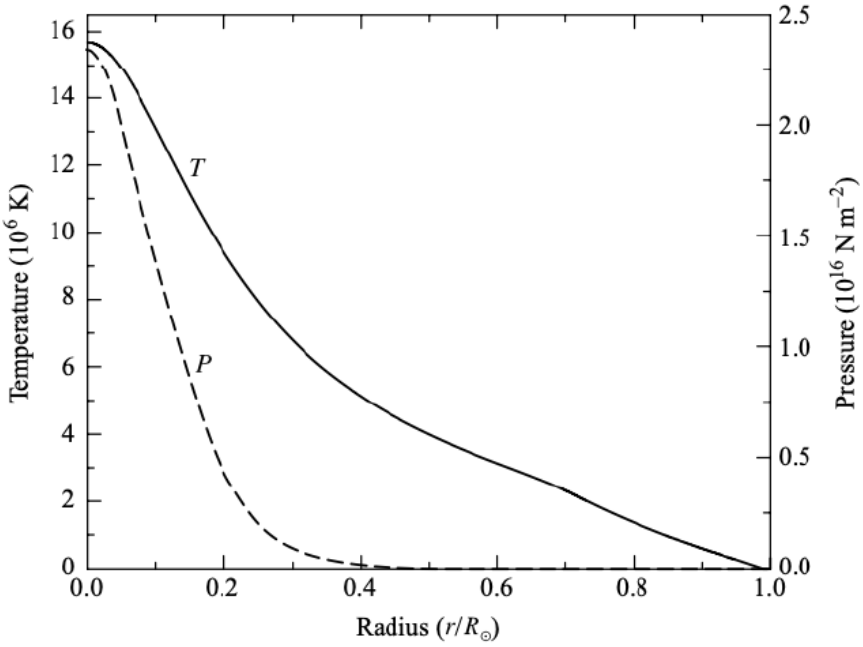

Figure 2: Plot of Temperature T and Pressure P vs r (Data from Bahcall, Pinsonneault, and Basu, Ap. J, 555, 990, 2001.) (Carroll & Ostlie, 2017)

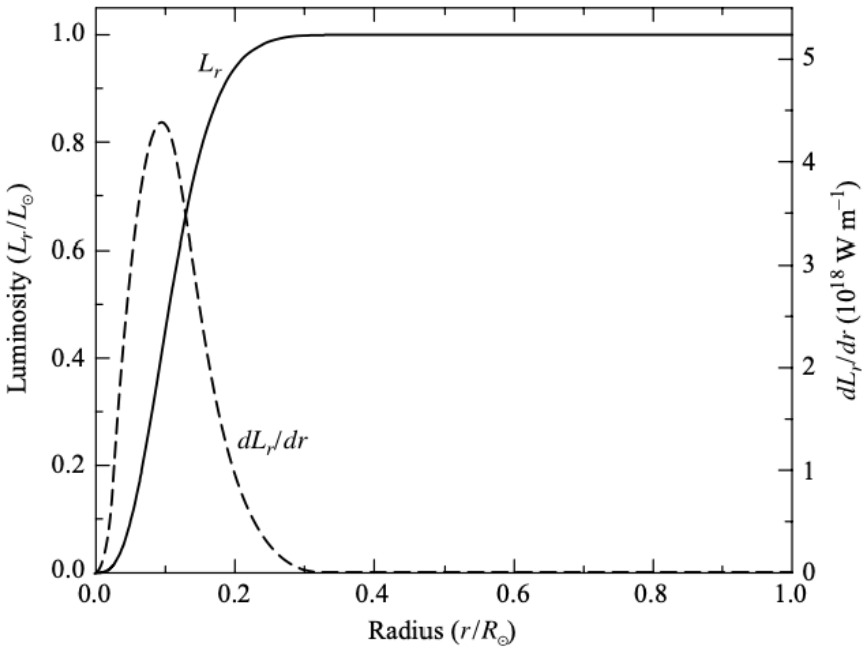

Figure 3: Plot of interior Luminosity profile L_r and its derivative with respect to r, as a function of r (Data from Bahcall, Pinsonneault, and Basu, Ap. J, 555, 990, 2001.) (Carroll & Ostlie, 2017)

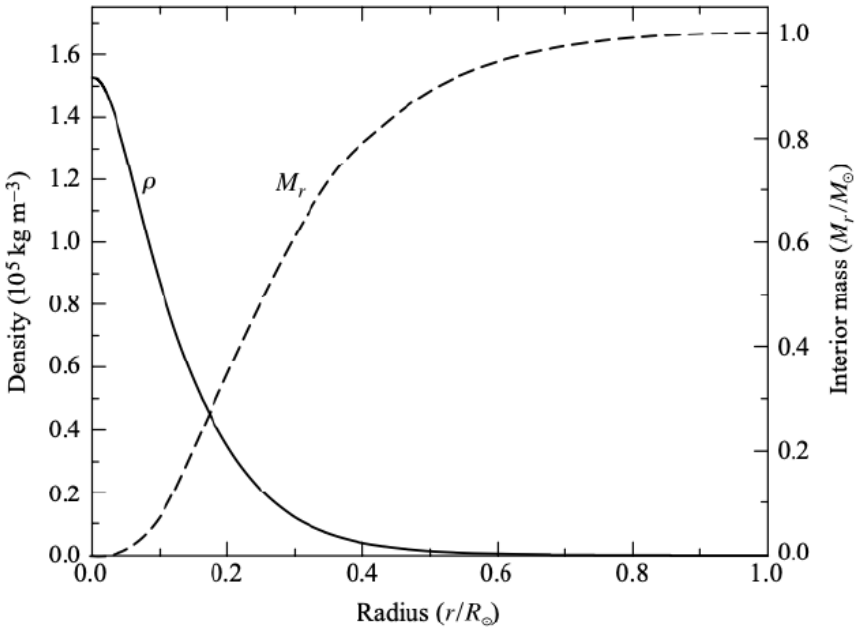

Figure 4: Plot of ρ vs r (Data from Bahcall, Pinsonneault, and Basu, Ap. J, 555, 990, 2001.) (Carroll & Ostlie, 2017)

4 Helioseismology

We now study an alternate method to probe the interior of the sun directly through the study of stellar oscillations - helioseismology (Basu & Chaplin, 2017):

4.1 Equations of Fluid Dynamics

We will model our stellar material as a fluid under the presence of a gravitational potential.

1. **Continuity Equation:**

$$\frac{\partial \rho}{\partial t} + \nabla \cdot (\rho \mathbf{v}) = 0 \tag{4.1}$$

   where $\mathbf{v}$ is the velocity of a fluid element.

2. **Momentum Equation**

$$\rho \left(\frac{\partial \mathbf{v}}{\partial t} + \mathbf{v}(\nabla \cdot \mathbf{v}) \right) = -\nabla P + \rho \nabla \Phi \tag{4.2}$$

   where Φ is the gravitational potential.

3. **Poisson's Equation**

$$\nabla^2 \Phi = 4\pi G \rho \tag{4.3}$$

4. **Energy Equation in Adiabatic Approximation**

$$\frac{\partial P}{\partial t} + \mathbf{v}.\nabla P = c_s^2 \left(\frac{\partial \rho}{\partial t} + \mathbf{v}.\nabla \rho \right) \tag{4.4}$$

   where we have the speed of sound

$$c_s = \sqrt{\frac{\Gamma_1 P}{\rho}} \tag{4.5}$$

   where $\Gamma_1 = (\partial \ln P / \partial \ln \rho)_{ad}$.

4.2 Perturbed Form

To study oscillations, we must first perturb the stellar material from it's equilibrium position. For instance, for ρ, we can write

$$\rho(\mathbf{r}, t) = \rho_0(\mathbf{r}) + \rho_1(\mathbf{r}, t) \tag{4.6}$$

Using the Lagrangian perturbation we have

$$\delta\rho(\mathbf{r}, t) = \rho(\mathbf{r} + \xi(\mathbf{r}, t)) - \rho(\mathbf{r}) = \rho_1(\mathbf{r}, t) + \xi(\mathbf{r}, t) \cdot \nabla \rho_0 \tag{4.7}$$

where ξ is the displacement from equilibrium position, and velocity is $d\xi/dt$.

Substituting the perturbed quantities in 4.1, 4.2, 4.3, and 4.4, and keeping only the linear terms in perturbation,

$$\rho_1 + \nabla \cdot (\rho_0 \vec{\xi}) = 0 \tag{4.8}$$

$$\rho_0 \frac{\partial^2 \vec{\xi}}{\partial t^2} = -\nabla P_1 + \rho_0 \nabla \Phi_1 + \rho_1 \nabla \Phi_0 \tag{4.9}$$

$$\nabla^2 \Phi_1 = 4\pi G \rho_1 \tag{4.10}$$

$$P_1 + \vec{\xi} \cdot \nabla P_0 = c_0^2 (\rho_1 + \vec{\xi} \cdot \nabla \rho_0) \tag{4.11}$$

In future references to these equations we drop the subscript 0 for equilibrium quantities and retain only the subscripts for perturbed quantities.

4.3 Spherically Symmetric Solutions

In our case of spherical symmetry, the perturbed equations can be factored into radial (r), tangential (θ, ϕ) and temporal parts. Solutions to the tangential parts are given by the spherical harmonic functions:

$$Y_l^m(\theta, \phi) = \sqrt{\frac{(2l+1)}{4\pi} \frac{(l-m)!}{(l+m)!}} P_l^m(\cos\theta) e^{im\phi} \tag{4.12}$$

where P_l^m denote the Legendre polynomials. Thus we can write

$$\xi_r(r, \theta, \varphi, t) \equiv \xi_r(r) Y_l^m(\theta, \varphi) \exp(-i\omega t) \tag{4.13}$$

$$P_1(r, \theta, \varphi, t) \equiv P_1(r) Y_l^m(\theta, \varphi) \exp(-i\omega t) \tag{4.14}$$

and so on.

Using these in 4.8 we get

$$\frac{d\xi_r}{dr} = -\left(\frac{2}{r} + \frac{1}{\Gamma_1 P}\frac{dP}{dr}\right)\xi_r + \frac{1}{\rho c^2}\left(\frac{S_l^2}{\omega^2} - 1\right) P_1 - \frac{l(l+1)}{\omega^2 r^2}\Phi_1 \tag{4.15}$$

$$\frac{dP_1}{dr} = \rho\left(\omega^2 - N^2\right)\xi_r + \frac{1}{\Gamma_1 P}\frac{dP}{dr} P_1 + \rho \frac{d\Phi_1}{dr} \tag{4.16}$$

$$\frac{1}{r^2}\frac{d}{dr}\left(r^2 \frac{d\Phi_1}{dr}\right) = -4\pi G\left(\frac{P_1}{c^2} + \frac{\rho \xi_r}{g} N^2\right) + \frac{l(l+1)}{r^2}\Phi_1 \tag{4.17}$$

where we define the *lamb frequency*

$$S_l^2 = \frac{l(l+1)c^2}{r^2} \tag{4.18}$$

and the *Brunt-Väisälä frequency*:

$$N^2 = g\left(\frac{1}{\Gamma_1 P}\frac{dP}{dr} - \frac{1}{\rho}\frac{d\rho}{dr}\right) \tag{4.19}$$

Clearly, $N^2 < 0$ gives back the Schwarzschild Criterion.

Since the equations depend only on l, we can label the eigenvalues with same l with a free index n as $\omega_{n,l}$ where n can be any integer. The degree 'l' is related to the horizontal wavelength of the mode and is approximately the number of nodes on the solar surface. The azimuthal order m defines the number of nodes along the equator. Due to spherical symmetry, the nodes of given n, l are degenerate in m. We have

- $n > 0$: acoustic or p modes, as their restoring force is pressure
- $n = 0$: fundamental mode
- $n < 0$: gravity or g modes, as their restoring force is gravity through buoyancy

4.4 Final Oscillatory Form

Now approximating equations 4.15 onward, we can assert the following simplifications:

- Cowling approximation: perturbation to the gravitational potential Φ_1 can be ignored where $|n|$ and l are large
- We assume that we are looking far away from center (i.e. large l) so $1/r$ terms are neglected,
- We assume that variations in eigenfunctions is more rapid than equilibrium quantities for high $|n|$ oscillations hence terms containing H_P^{-1} can be neglected, where $H_P = -\frac{dr}{d\ln P}$ is the pressure scale height.

Thus we finally get

$$\frac{d^2\xi_r}{dr^2} = K(r)\xi_r \tag{4.20}$$

where

$$K(r) = \frac{\omega^2}{c^2}\left(1 - \frac{N^2}{\omega^2}\right)\left(\frac{S_l^2}{\omega^2} - 1\right) \tag{4.21}$$

For the solution to be oscillatory we need the kernel K to be negative. Thus we have

- $\omega^2 < S_l^2$, and $\omega^2 < N^2$: **g** modes - trapped mainly in the core - restoring force is gravity through buoyancy,
- $\omega^2 > S_l^2$, and $\omega^2 > N^2$: **p** modes - generally oscillatory in outer regions restoring force is mainly pressure;

These conditions can be clearly depicted in Figure 6.

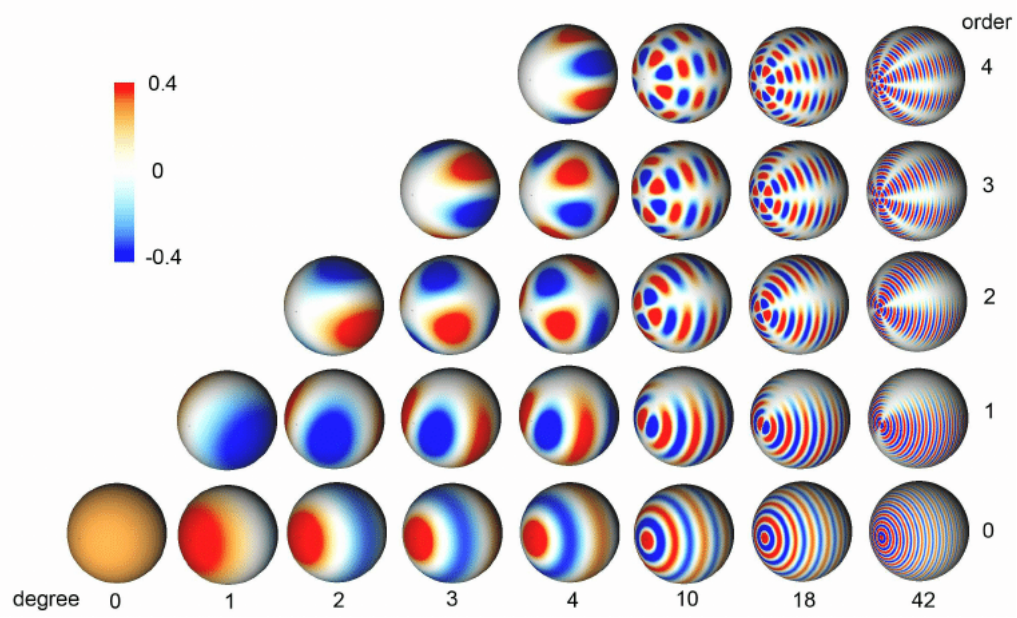

Figure 5: Various spherical harmonics $Y_l^m(\theta,\ \phi)$ (Chung et al., 2008)

One important result we get is that we can calculate the frequency of different modes using observable quantities such as surface velocities, sound speed profile and the *Brunt-Väisälä frequency*(Basu & Chaplin, 2017). Thus, we can analyse the effects of g-modes further in the report without having to rely on solar models that make assumptions about the density profiles etc.

4.5 p modes

The p -modes are trapped between the surface and the inner turning point r_t given by $\omega^2 = S_l^2$. For high frequency p modes, i.e., modes with $\omega \gg N^2$

$$K(r) \simeq \frac{\omega^2 - S_l^2(r)}{c^2(r)} \tag{4.22}$$

hence, their behavior is predominantly determined by the behavior of the sound-speed profile, which is pressure, i.e., sound waves ($n > 0$).

Figure 10 shows the non-radial p -modes for different degree and order. We observe that lower degree modes penetrate deeper into the core whereas higher degree modes have significant amplitude of oscillation close to the stellar-surface only. Thus, they allow a diagnosis of the conditions on the surface layers.

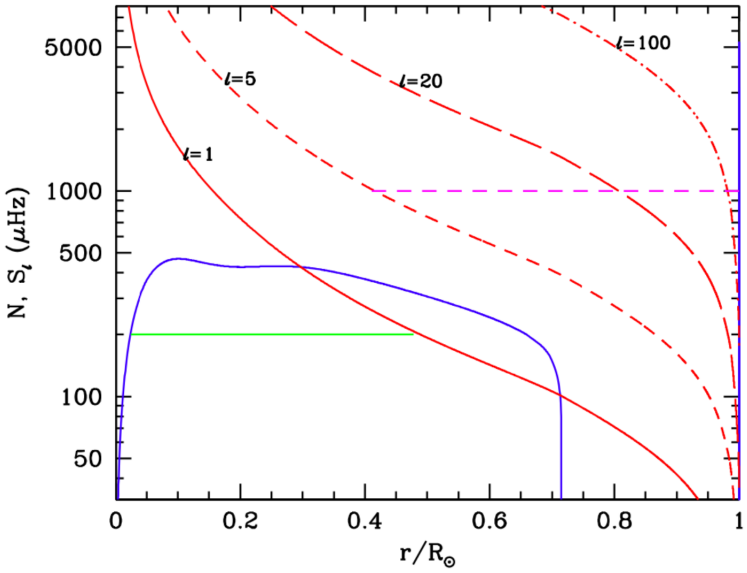

Figure 6: The propagation diagram for a standard solar model. The blue line is the buoyancy frequency, the red lines are the Lamb frequency for different degrees. The green solid horizontal line shows the region where a 200 μHz g-mode can propagate. The pink dashed horizontal line shows where a 1000 μHz l = 5 p-mode can propagate. (Basu, 2016)

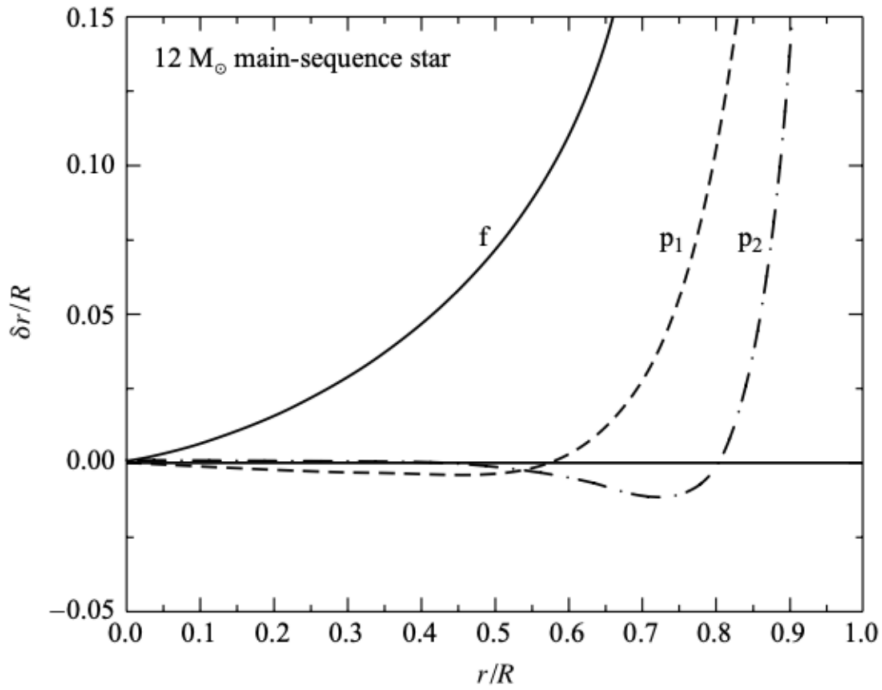

Figure 7: $l = 2$ and f mode is shown for 12 $M_\odot$ star.. (Carroll & Ostlie, 2017)

4.6 g modes

In the case of the Sun the g modes are trapped between the base of the convection zone and the core. The turning points of these modes are defined by $N = \omega$. For g -modes of high order, $\omega^2 \ll S_l^2$ and thus

$$K(r) \simeq \frac{1}{\omega^2}\left(N^2 - \omega^2\right)\frac{l(l+1)}{r^2} \tag{4.23}$$

hence its properties are dominated by the buoyancy frequency N.$(n < 0)$

Now since g modes are trapped deep in the interior, they give us a good idea about the core properties which are essential when we are trying to study the abundances of metals, as well as nuclear reactions. Unfortunately they cannot be directly observed unlike p modes.

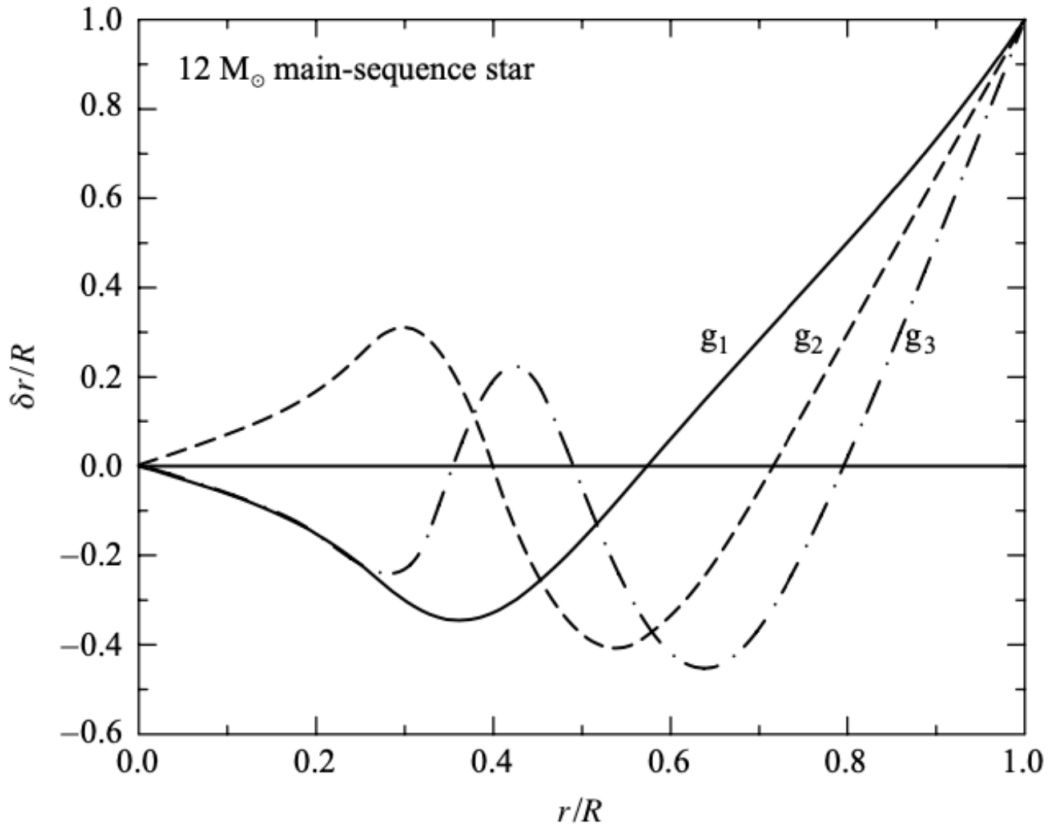

Figure 8: g modes with $l = 2$ (Carroll & Ostlie, 2017)

4.7 Helioseismic Inferences

We have 2 main methods for helioseismic inferences:

- **Forward Technique**: Compare frequencies of different models with observed frequencies. For e.g. estimating R_{CZ}- depth of the convection zone

- **Inverse technique**: Using the observed frequencies, infer the internal structure or dynamics. For e.g., sound speed profile $c(r)$.

4.7.1 Helioseismic Inversions

Since the frequencies of acoustic modes depend mainly on the sound speed and density in solar interior, it is possible to invert the frequencies of observable modes to obtain the sound speed c, and density ρ (Basu & Antia, 2008). It can be shown that c, ρ along with hydrostatic equilibrium are enough to determine the solar model as far as frequencies are concerned. Pressure p and adiabatic index Γ_1 can be determined from c, ρ.

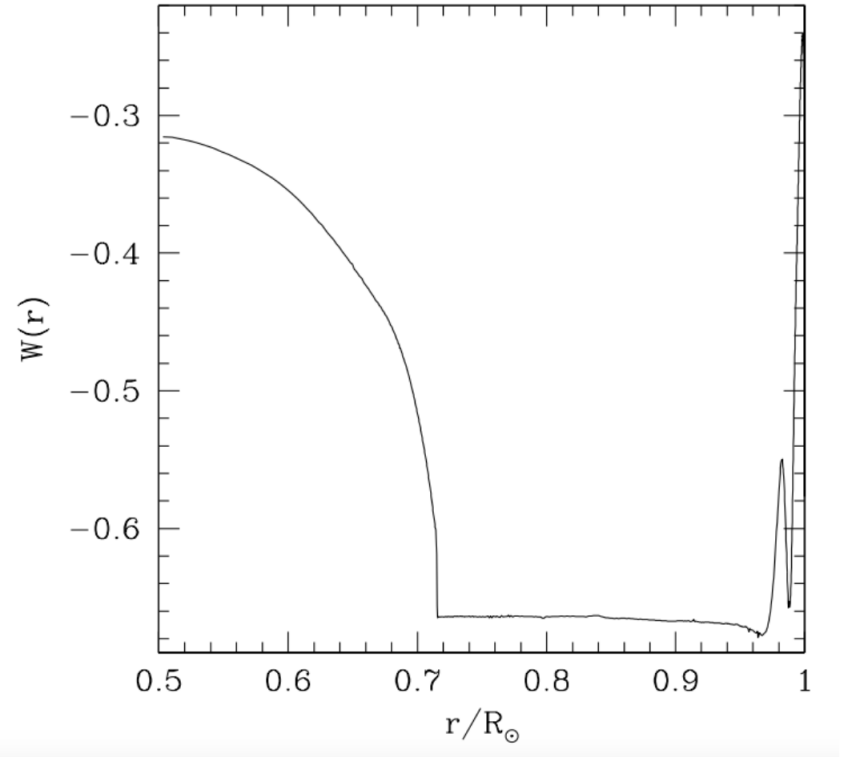

Figure 9: Variation of the dimensionless gradient of sound speed profile $W(r) = \frac{r^2}{Gm}\frac{dc^2}{dr}$ with r. The peak around $r \approx 0.98R_\odot$ is due to the $HeII$ ionization zone and can be calibrated to find helium abundance (Basu & Antia, 2008)

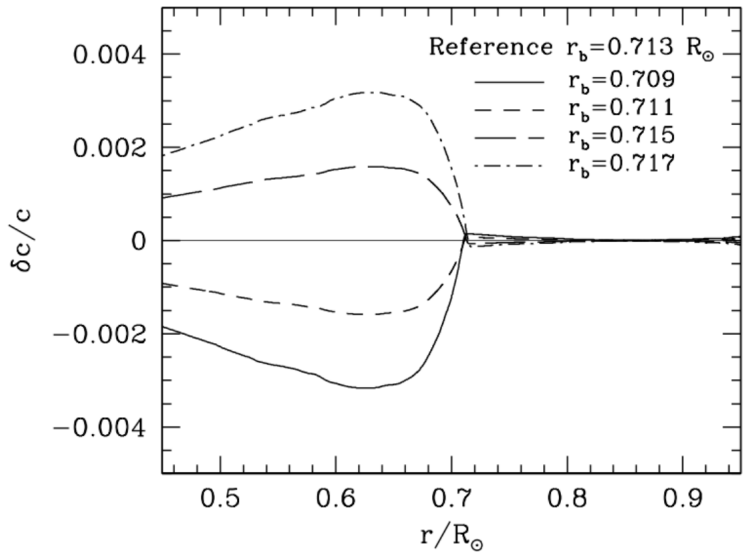

Figure 10: The discontinuity in the sound speed for different models show the position of the tachocline (Basu & Antia, 2008)

5 Beyond the Standard Solar Model

As seen earlier, the standard solar model tunes some unknown parameters such as the initial chemical composition, mixing length to fit the known parameters such as solar mass, radius, luminosity etc.
We now rewrite the equations of the standard solar model as:

$$\frac{dP}{dr} = -\frac{GM\rho}{r^2} \tag{5.1}$$

$$\frac{dM}{dr} = 4\pi r^2 \rho \tag{5.2}$$

$$\frac{dL}{dr} = 4\pi r^2 \rho \left(\epsilon + \epsilon_{gr} - \epsilon_{\nu}\right) \tag{5.3}$$

$$\frac{dT}{dr} = -\frac{3\kappa\rho L}{16\pi r^2 \alpha T^3}, \qquad \nabla_{\text{rad}} < \nabla_{\text{ad}} \tag{5.4}$$

$$= \nabla_{ad} . \frac{T}{P}\frac{dP}{dr}, \qquad \nabla_{\text{rad}} > \nabla_{\text{ad}} \tag{5.5}$$

$a = 4\sigma$, $\nabla_{ad} = \left(\frac{\partial \ln T}{\partial \ln P}\right)_S$ and $\nabla_{rad} = \frac{3\kappa LP}{16\pi aGMT^4}$. The equation of heat transfer in the core 5.4 is a form of the Fick's equation.
In the convective zone, except in the outermost layers, we can approximate the equation of state as the ideal gas law: $P = \frac{\rho T}{\mu m_H}$, where m_H is the proton mass, μ is mean molecular weight normalized to proton mass, and the Boltzmann constant has been set to unity.

$$\mu = \frac{\Sigma_j n_j A_j}{\Sigma_j n_j (1+Z_j)} = \left[\Sigma_j \frac{X_j}{A_j}(1+Z_j)\right]^{-1} \simeq \left[2X + \frac{3Y}{4} + \frac{Z}{2}\right]^{-1} \tag{5.6}$$

From the ideal gas law and 5.1, we get

$$T \sim \frac{\mu P}{\rho} \sim \frac{\mu GM}{R} \tag{5.7}$$

Substituting in 5.4

$$L \sim \frac{R^2}{\kappa\rho}\left(\frac{T^4}{R}\right) \sim \frac{\mu^4 M^3}{\kappa} \tag{5.8}$$

Substituting the mean molecular weight,

$$\mu \simeq \frac{4}{8-5Y-6Z} \implies \frac{M^3}{L} \simeq \kappa(8-5Y-6Z)^4 \tag{5.9}$$

Thus, since the mass and luminosity are fixed, any opacity change must majorly depend on a change in Helium abundance.
The old GS98 model of solar abundances was replaced by the AGSS09 model which better explained the solar spectrum and whose discrepancies with respect to GS98 were well understood. However, the decreased metallicity in AGSS09 dataset gives wrong results with the Standard Solar Model.
As seen earlier, the process of Helioseismic inversion of frequency spectra allows us to gauge the unknown parameters in the Standard Solar model decently accurately, and these conflict with the results from the Standard Solar Model. The main discrepancy is in the sound speed profiles in the solar radiative zone.

6 Non-Diffusive Energy Transport Solution

One of the easiest proposed solutions to the solar abundance problem is to increase the opacity profile in the solar radiative zone (Sokolov, 2020).
The non-diffusive energy transport solution considers an analogue of radiative transport, since convective transport in the radiative zone of the sun is inconsistent with Helioseismic data. This can be implemented by emission of some unknown particles from one region of the sun, their propagation/transport in the sun and subsequent energy transfer to another region of the sun.
This will result in additional terms in 5.3, which may have positive or negative sign.
Shifting from radial to mass coordinates, where primed quantities are mass derivatives:

$$m \equiv M/M_\odot,\ \tilde{r} \equiv r/R_\odot,\ \tilde{\rho} \equiv \rho/\rho_0,\ \tilde{p} \equiv P/P_0,\ \tilde{l} \equiv L/L_\odot,\ \tilde{t} \equiv T/T_0,\ \tilde{\kappa} \equiv \kappa/\kappa_0,\ \tilde{\epsilon} \equiv \epsilon/\epsilon_0$$

where

$$\rho_0 \equiv \frac{M_\odot}{\frac{4}{3}\pi R_\odot^3},\ \ P_0 \equiv \frac{2}{3}\pi R_\odot^2 G\rho_0^2,\ \ T_0 \equiv \frac{GM_\odot m_H}{R_\odot},\ \ \kappa \equiv 1.0\ \ cm^2/g,\ \ \epsilon_0 \equiv 1.0\ \ erg/g.s$$

Rewriting the solar equations in this form:
Hydrostatic equilibrium:

$$p' = -\frac{2m}{3r^4} \tag{6.1}$$

Continuity equation:

$$r' = \frac{1}{3\rho r^2} \tag{6.2}$$

Energy production equation:

$$l' = \xi_1 \left(\epsilon_{nuc} - \epsilon_\nu + \sum_i \epsilon_i \right) \tag{6.3}$$

Energy Transport equation (Fick's Law):

$$t' = -\xi_2 \frac{\kappa l}{r^4 t^3} \tag{6.4}$$

Equation of state:

$$p = 2\frac{\rho t}{\mu} \tag{6.5}$$

where the numerical coefficients ξ_1 and ξ_2 are defined as follows:

$$\xi_1 \equiv \epsilon_0 \frac{M_\odot}{L_\odot} \sim 0.52,\ \ \xi_2 \equiv \frac{3}{64\pi^2 a} \frac{\kappa_0 L_\odot M_\odot}{(GM_\odot m_H)^4} \sim 2.4 \times 10^{-5} \tag{6.6}$$

In 6.3, the contribution of ϵ_{gr} is small and has been neglected. The terms ϵ_i correspond to non-diffusive energy transport.
In finding the luminous flux power, we can use the constraint of the results which are correct

from the standard solar model. Since the surface luminosity is fixed and has already been characterized by the terms of nuclear emission and neutrino energy losses,

$$\xi_1 \int_0^1 [\epsilon_{nuc}(m) - \epsilon_\nu(m)]_{SSM} dm = 1 \tag{6.7}$$

where the subscript 'SSM' denotes that the function has been evaluated in the Standard Solar Model's framework.
Finally, we can split the additional terms in the energy production equation as

$$\sum_i \epsilon_i = \sum_i \tilde{\epsilon}_i + \bar{\epsilon}, \;\; \bar{\epsilon} \equiv \int_0^1 dm \sum_i \epsilon_i \tag{6.8}$$

Then by definition $\int_0^1 dm \sum_i \tilde{\epsilon}_i = 0$. This determines the part corresponding to non-diffusive energy transport, and $\bar{\epsilon}$ corresponds to the total power generated in solar plasma by unknown sources or lost by the plasma through unknown sinks.

Let us denote look at any quantity x in the standard solar model, and a model which incorporates an additional energy transport term, and denote the difference in the value of the quantity between the models by δx.
Starting with equations 6.4 and 6.1, we get

$$l \propto \frac{mt^3 t'}{\kappa p'} \tag{6.9}$$

Using the opacity tables such as OPAL, we can write $\kappa \propto \rho^\alpha t^{-\beta}$ for some $\alpha,\ \beta$.
Now using $c_s^2 \propto p/\rho \propto t/\mu$ (where the second proportionality comes from ideal gas law), we get

$$\frac{\delta t}{t} = 2\frac{\delta c_s}{c_s} + \frac{\delta \mu}{\mu} \tag{6.10}$$

From allowed errors in observed data, we can conclude that the considered variations of density, sound speed, temperature and sound speed profile are much less than unity, validating the approximations of the variational method. Similarly, it can be shown that the variation in p' is much less than unity.
Then, writing t' and p' in terms of helioseismic observables:

$$\frac{\delta(t')}{t'} = \frac{(\delta t')}{t'} = \frac{t}{t'}\left(\frac{\delta t}{t}\right)' + \frac{\delta t}{t} = 2\frac{t}{t'}\left(\frac{\delta c_s}{c_s}\right)' + \frac{t}{t'}\left(\frac{\delta \mu}{\mu}\right)' + 2\left(\frac{\delta c_s}{c_s}\right) + \frac{\delta \mu}{\mu} \tag{6.11}$$

and

$$\frac{\delta p'}{p'} = \frac{p}{p'}\left(\frac{\delta p}{p}\right)' + \frac{\delta p}{p} = \frac{p}{p'}\left(\frac{\delta \rho}{\rho}\right)' + 2\frac{p}{p'}\left(\frac{\delta c_s}{c_s}\right)' + 2\frac{\delta c_s}{c_s} + \frac{\delta \rho}{\rho} \tag{6.12}$$

Substituting the above results into the solar luminosity variation:

$$\frac{\delta l}{l} = 2(3+\beta)\frac{\delta c_s}{c_s} - (1+\alpha)\frac{\delta \rho}{\rho} + (4+\beta)\frac{\delta \mu}{\mu} + \frac{t}{t'}\left[2\left(\frac{\delta c_s}{c_s}\right)' + \left(\frac{\delta \mu}{\mu}\right)'\right] - \frac{p}{p'}\left[\left(\frac{\delta \rho}{\rho}\right)' + 2\left(\frac{\delta c_s}{c_s}\right)'\right] \tag{6.13}$$

Since the helioseismic inversions as well as SSM have their errors, it is not straightforward to calculate $\delta l/l$ profile and fix a shape for the required variation. To fix the shape, results from a hypothetical solution of direct variation of opacity is used.

6.1 Model - Direct Opacity Shift

The SSM involves several numerical integration steps of Non-Linear partial differential equations which makes it hard to correctly interpret changes. Thus, the author of Villante (2010a) paper developed a linear solar model (Villante, 2010b) to investigate the role of parameters and assumptions more efficiently.
Take opacity $\kappa(\rho, T, Y, Z_i)$. Consider the effect of metallicity only in the equation of state of the radiative transport in the sun. Then, the AGSS09 metallicity implies a total variation in the opacity profile as:

$$\delta\kappa^{tot}(r) = \frac{\kappa(\rho(r), T(r), Y(r), Z_i(r)}{\bar{\kappa}(\bar{\rho}(r), \bar{T}(r), \bar{Y}(r), \bar{Z}_i(r)} - 1 \tag{6.14}$$

where the barred terms refer to SSM values, while unbarred terms refer to varied values. This model will now assume the following

- Performed changes in opacity and heavy element admixture is small
- Variation of chemical composition can be estimated from variation of nuclear reaction rate and diffusion efficiency
- Variation of metal admixture has negligible direct effect on nuclear production of He and on diffusion efficiency

Simplifying the above equation

$$\delta\kappa^{tot}(r) = \kappa_T\delta T(r) + \kappa_\rho\delta\rho(r) + \kappa_Y\Delta Y(r) + \sum_i \kappa_i\delta Z_i(r) + \delta\kappa_I(r) \tag{6.15}$$

Here, $\delta\kappa_I$ is an intrinsic change in opacity function, and the rest of the terms correspond to the effect of changes in other parameters. The coefficients are:

$$\kappa_T = \frac{\delta \ln \kappa}{\delta \ln T}\|_{SSM} \qquad \kappa_\rho = \frac{\delta \ln \kappa}{\delta \ln \rho}\|_{SSM}$$
$$\kappa_Y = \frac{\delta \ln \kappa}{\delta Y}\|_{SSM} \qquad \kappa_i = \frac{\delta \ln \kappa}{\delta \ln Z_i}\|_{SSM}$$

Now, using the ideal gas equation we can simplify the equation by substituting

$$\delta\rho = \delta P(r) - \delta T(r) - P_Y(r)\Delta Y(r) \tag{6.16}$$

Where $P_Y(r) = -\frac{\delta \ln \mu}{\delta Y} \simeq -\frac{5}{8-5Y(r)}$. Then substituting the same, and substituting $\delta Z_i(r)$ and $\Delta Y(r)$ from the LSM,

$$\delta\kappa^{tot}(r) = \kappa'_T\delta T(r) + \kappa'_P\delta P(r) + \kappa'_Y\Delta Y_{ini} + \kappa_c\delta C + [\delta\kappa_I(r) + \delta\kappa_Z(r)] \tag{6.17}$$

κ_Z is the composition opacity change, given by $\delta\kappa_Z(r) = \sum_i \kappa_i\delta z_i$.

$$\kappa'_T = \kappa_T - \kappa_\rho(1 + P_Y\xi_T) - K_Y\xi_T$$
$$\kappa'_P = \kappa_\rho(1 - P_Y\xi_p) - K_Y\xi_P$$
$$\kappa'_Y = (\kappa_Y - \kappa_\rho P_Y)\xi_Y + Q_Y\kappa_Z\kappa_C = Q_C\kappa_Z$$

The coefficients Q_h and ξ_h are given by detailed calculations of the solar composition in the LSM, which is covered in Villante (2010b).
In 6.17, the parts not in square brackets [ ] can be derived, however, the part in [ ] can, in principle, be varied in any way. Thus, we must set bounds based on observational data.
Thus, this approach finds variation in opacity based on the equations of state of the solar model, and fitting data to observations. This opacity will differ from the opacity values calculated by OPAL and others, which were derived by theoretical modelling of inter-particle interactions at the various densities and temperatures, which gives singular points which can be interpolated to form functions for the SSM.

Coming back to the luminosity variation, $\bar{\delta}$ refers to variation in the B16 SSM with respect to this shifted opacity model. This gives the final results:

$$(\delta l)_{add} = l\times\left(\frac{\bar{\delta}\kappa}{\kappa} + 2\beta\frac{\delta c_s}{c_s} - \alpha\frac{\delta\rho}{\rho} + \beta\frac{\bar{\delta}\mu}{\mu} + (4+\beta)\left(\frac{\delta\mu}{\mu}\right)_{nuc} + \frac{t}{t'}\left(\frac{\delta\mu}{\mu}\right)'_{nuc} + \left(\frac{\bar{\delta}l - \delta l}{l}\right)_{nuc}\right) \tag{6.18}$$

Using this, we will discussed the results in case of $\bar{\epsilon} = 0$ and $\bar{\epsilon} \neq 0$

6.2 Results: $\bar{\epsilon} = 0$

In this case,

$$(\delta l)_{nuc} = (\bar{\delta} l)_{nuc} \text{ If } \bar{\epsilon} = 0$$

The sun does not lose or gain any additional energy. Then, 6.18 simplifies to

$$(\delta l)_{add} = l \times \left(\frac{\bar{\delta}\kappa}{\kappa} + 2\beta\frac{\delta c_s}{c_s} - \alpha\frac{\delta\rho}{\rho} + \beta\frac{\bar{\delta}\mu}{\mu}\right) \tag{6.19}$$

Here, from 5.9, we can relate the quantity $\bar{\delta}\mu$ with the helioseismological surface helium abundance. The variation $\bar{\kappa}$ is taken from the reference of section 6.1. Using this opacity and the relations $\kappa \propto \rho^{\alpha} t^{-\beta}$, and $c_s \propto p/\rho \propto t/\mu$, we obtain the remaining terms.
Note that since the formula uses Fick's Law, it is only valid in the radiative zone.
Since the SSM assumes effective convective mixing in the convective zone, and agrees with Helioseismology data, we cannot significantly change the energy transport terms without contradictions.
Thus, according to the plot, we require emission on particles at the boundary of convective zone, and some source of heating within approximately $r \in [0.1, 0.3]$.
If we are interested in reconciliation of sound speed profile (since global rescaling of opacity does not influence it), we can add an arbitrary constant to the RHS of 6.18. This resembles the solution of the anomaly provided by dark matter diffusive energy transport.
Numerically, the case of C = -0.26 results in the required additional energy transfer from the centre of the solar core to its periphery.

6.3 Results: $\bar{\epsilon} \neq 0$

The additional 3 terms in 6.18 have been estimated earlier.
The case of $\bar{\epsilon} = -0.2$, which corresponds to maximum allowed energy loss through solar

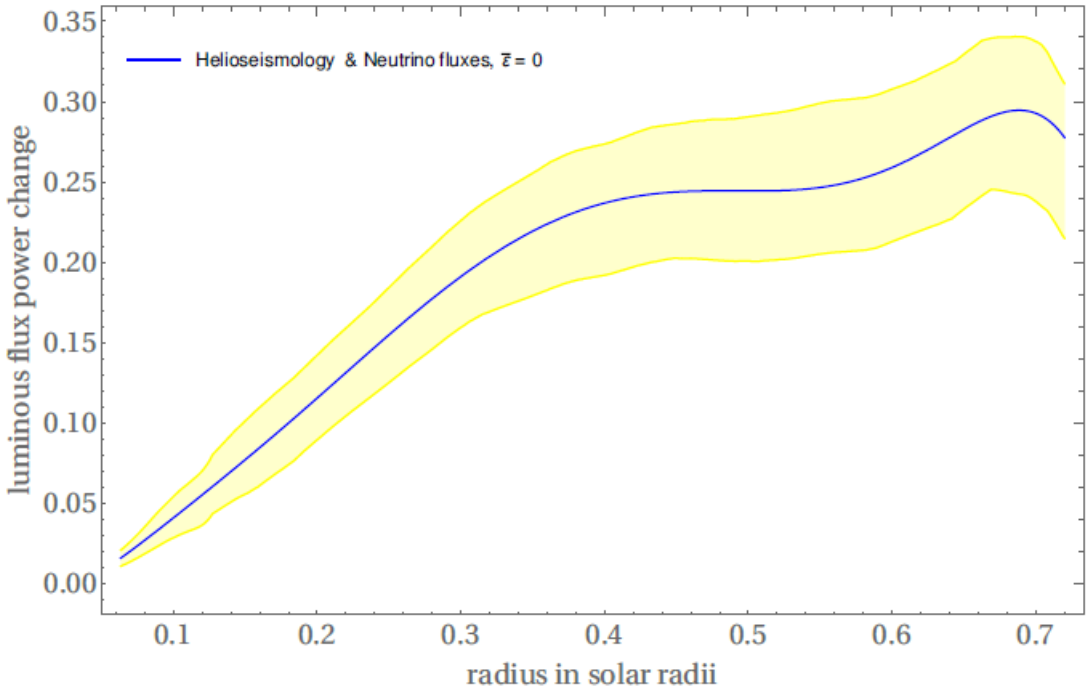

Figure 11: Additional power of luminous flux $(\delta l)_{add}$, which solves the solar abundance problem, as a function of radial coordinate inside the core and radiative zone, $\bar{\epsilon} = 0$ (Sokolov, 2020)

neutrino data, gives a requirement of the required power being dominantly positive (Fig 13). However, if we were to try to solve the solar abundance problem by loss of energy alone, the additional power profile would need to be non-positive.

Analogously, the case $\bar{\epsilon} > 0$ requires $(\delta l)_{add} > 0.2$, whereas the solar neutrino data allows a maximum $l_{gain} < 0.1$. Thus, although some limited loss or gain of energy by the Sun is allowed in principle, the resulting addition to the power profile becomes wavy in the core, making it hard to find a real physical model to explain the same.

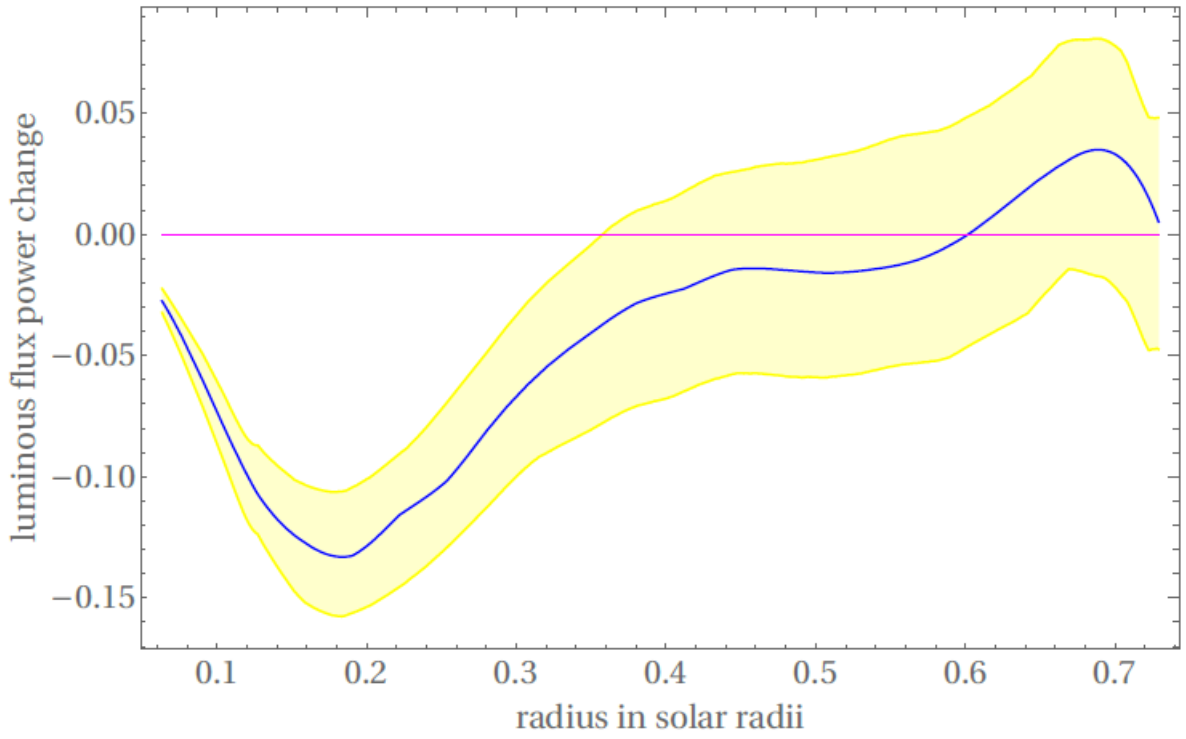

Figure 12: Additional power of luminous flux, which gives the helioseismological sound speed profile, as a function of radial coordinate inside the core and radiative zone, $\bar{\epsilon} = 0$, $C = -0.26$ (Sokolov, 2020)

7 Particle Physics Model

One possible solution to the requirement of localized emission of energy at the boundary of radiative zone can be some resonant processes due to mixing of WISPS with photons (Sokolov, 2020). In particular, in case of hidden photons, the resonant conversion occurs whenever the thermal photon mass ω_{pl} is equal to the hidden photon mass $m_{\gamma'}$ or the hidden photon energy $\omega_{\gamma'}$, depending on the polarization of hidden photon.
Assumptions:

- Additional U(1)' gauge symmetry
- Mass of hidden photon $m_{\gamma'} \neq 0$.
- Mass mixing parameter is negligible compared to kinetic mixing

For resonant production of longitudinally polarized hidden photons, we need $\omega_{pl} \geq m_{gamma'}$, which is a large region inside the sun. These hidden photons will have some definite energy. For production of transversely polarized hidden photons, the resonant production will only occur in a thin spherical shell of width $\sim 10^{-4}\ R_{\odot}$. Such a narrow region of resonant emission near the solar convective zone is exactly what we need. Using the condition $m_{gamma'} = \omega_{pl}(r = 0.7) = 12eV$. In this scenario, the resonant production of longitudinally polarized hidden photons will be negligible.

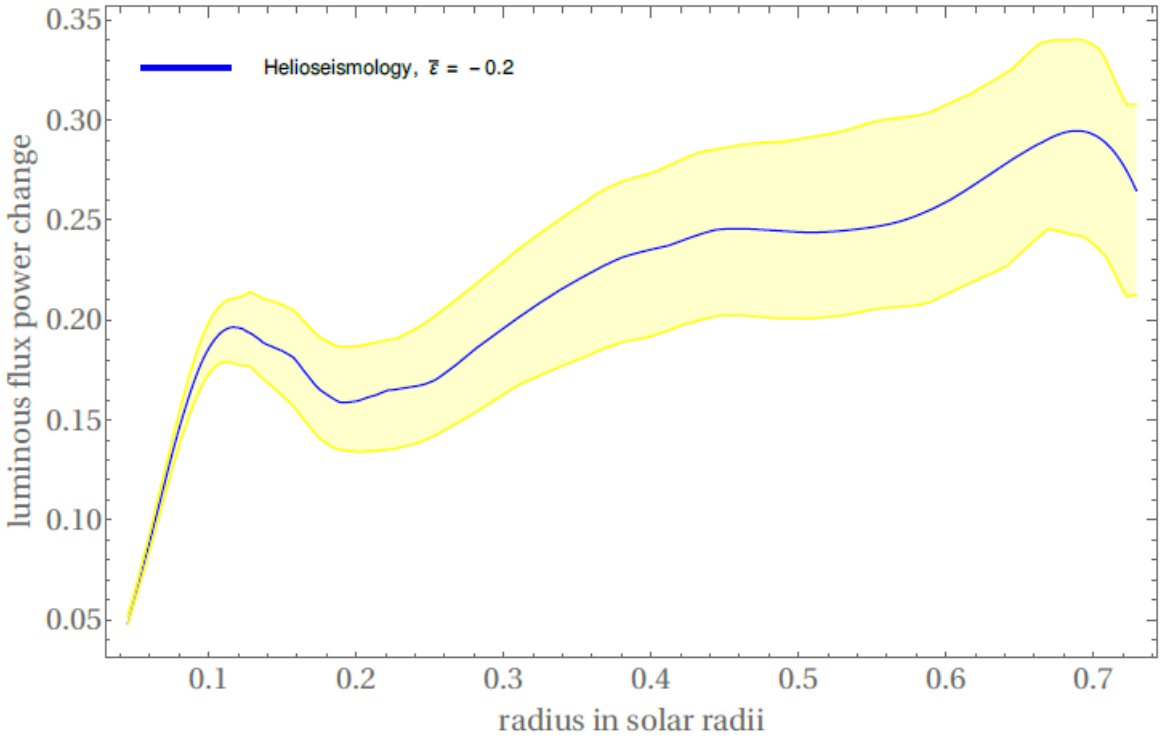

Figure 13: Required $(\delta l)_{add}$ to the power of luminous flux as a function of radial coordinate, $\bar{\epsilon} = -0.2$. This shows that additional loss of energy alone cannot be a solution to the solar abundance problem. (Sokolov, 2020)

To obtain the required $\Delta(\delta l) \simeq -0.26$, we need the kinetic mixing parameter $\chi \simeq 1.5 \times 10^{-13}$. These values do not contradict any existing laboratory or astrophysical constraints. However, we still need to ensure that the total energy loss $l_{loss} < 0.1$.

7.1 Millicharged particles

In case the energy scale of interaction and mass parts of Lagrangian (of the regular and hidden photons and their interaction with the electromagnetic field, various gauge fields and external currents (of both SM and hidden sector)) is larger than the hidden photon mass, the hidden sector particles acquire an effective millicharge.
Thus, we consider the decay of a hidden photon into two millicharged fermions ($2m_c < m'_\gamma$). In case the gauge coupling constant of the hidden sector, e', is $\gtrsim 10^{-6}$, the distance travelled by the hidden photon before its decay is negligibly small compared to the solar scale. This allows us to consider the region of production of millicharges in the sphere with great accuracy.

7.1.1 Capture of millicharged particles

The magnetic field inside the solar core is confined within it, since the solar core rotates as a rigid body. The boundary between the rigid rotation of the core and the highly non-uniform convective zone is very thin by the solar scale. Thus, we can consider the sun to have a toroidal magnetic field.
For the allowed values of millicharge (from astrphysics) $\varepsilon \lesssim 10^{-14} - 10^{-13}$, the Larmor radius of the millicharged particles is very small. This means the produced millicharges are captured within the magnetic fields in the solar core and are captured in the solar interior.

7.2 Solar Plasma Heating

For the millicharged particles to heat the solar plasma, the temperature of the gas of the dark sector particles needs to be higher than the solar plasma temperature ($\equiv 1$ keV. This is much higher than the average energy of the millicharged particles near the radiative boundary.
A proposed mechanism for the same is the presence of some stable heavy dark particles,gravitationally bound in the solar core.If these are charged under the hidden $U(1)'$ group and radiate dark photons, the required energy could be obtained. However, this has not been studied in detail. The main process contributing to the energy transfer from millicharged particles to solar plasma is the process of Coulomb scattering of millicharges on electrons. Considering the millicharged particles to be fermions, considering their low millicharge as a reason to approximate the interactions to be like compton scattering, and using some constraints developed by other authors studying the supernova SN1987, we get the following relation of energy transfer Q:

$$Q = 1.6\frac{\text{erg}}{\text{s.cm}^3} \times \left(\frac{\varepsilon}{7\times10^{-15}}\right)^2 \left(\frac{\omega_{pl}}{290\text{eV}}\right)^2 \left(\frac{T_c}{\text{keV}}\right)^3 \left[\frac{T}{T_c} - 1\right] K\left(\frac{4T_c^2}{\omega_{pl}^2}\right) \tag{7.1}$$

where K(a) as a function of radial coordinate is given in fig. 14
The final result of the above calculations requires the magnetic field in the solar interior to be higher than current constraints. However, the current constraints depend on pressure excess calculations. If the pressure exhibited by the millicharge gas or other hidden processes is high enough, the magnetic field constraints can be relaxed. The authors (Sokolov, 2020) do not provide estimates on the same.

7.3 Conclusions of the Non-Diffusive Energy Transport Solution

- The variation of luminosity in non-diffusive energy transfer vs SSM with helioseismic values is not enough to provide a constrained answer. The addition of factors from the hypothetical opacity shift solution helps give a constraint on the required energy transfer.
- The results from this is production of energy at $r \in [0.1R_\odot, 0.3R_\odot]$ and deposition at radiation-convection boundary.

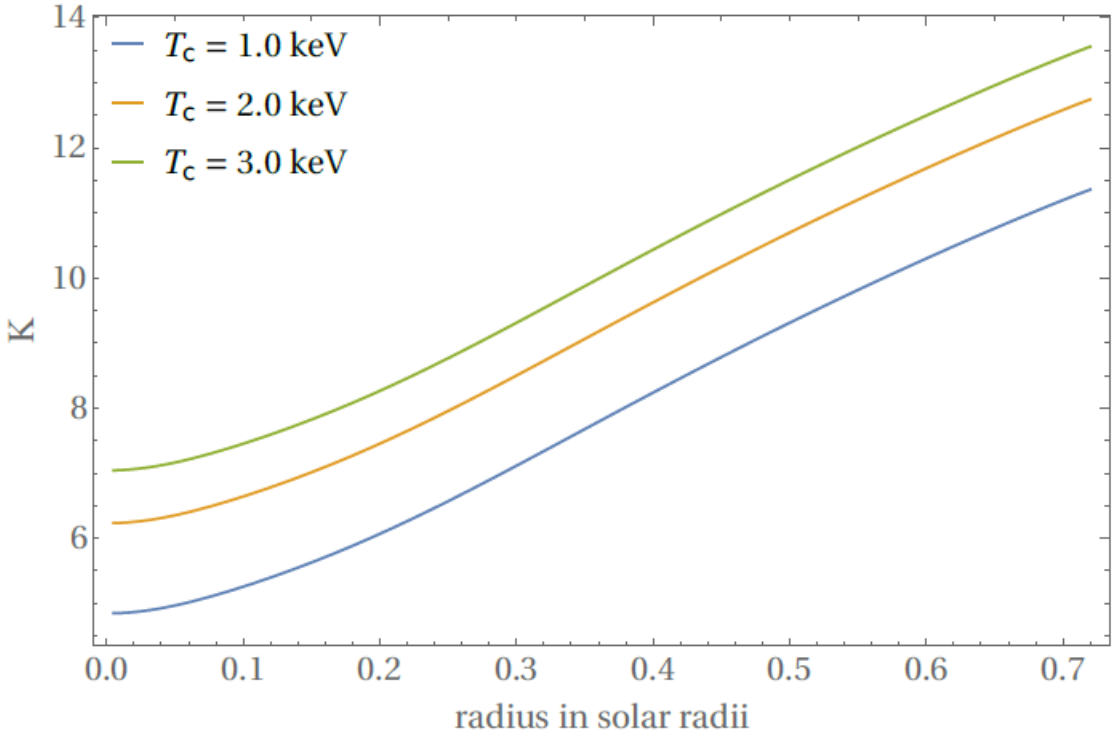

Figure 14: K(a) as a function of radial coordinate for the three values of temperature of the millicharged gas T_c (Sokolov, 2020)

- This is being explained by the presence of millicharged particles. It has been shown in the paper that particles of certain properties can be captured by the Sun's magnetic field. These can heat the core enough for production of dark photons which can achieve the required variation of luminosity in the radiative zone (however, not in the convective zone).
- The paper (Sokolov, 2020) did not well explain any mechanism to maintain the temperature of the light dark fermions within the sun.

As part of the research group, with the help of Prof. Rentala, Aman Awasthi, Siddhant Tripathy and B. Malavika, after discussing various possible solutions to the solar abundance problem, the group decided to pursue the study of solar g-modes to obtain accurate measurements of the properties in the solar core. In the rest of the report, I will be covering the current progress on probing solar g-modes using gravitational waves and gravitational wave detectors.

8 Gravitational Helioseismology

8.1 Introduction

- As mentioned earlier, the most common way of observing solar oscillation modes is by studying the doppler shift measurements of the time-dependent velocity of the surface of the sun.
- A number of detections of solar g-modes have also been reported, but these have low signal to noise ratio and are not mutually consistent. (Pallé, 1991)
- It has been claimed (but not universally accepted) that solar oscillations can be observed from the solar wind. Some frequencies observed in the solar wind correspond closely to known p mode frequencies and others are close to predicted g-mode frequencies - (Thomson et al., 1995)
- There have also been studies of the mixing of modes where the frequencies of low order p-modes get shifted due to mixing with g-modes, giving us an observable result. (Fossat et al., 2017)
- The upcoming space based gravitational wave detector LISA is designed to detect tiny gravitational wave frequencies in the range 10^2 to 10^6 μHz (Amaro-Seoane et al., 2017). Along with these far field observations, LISA will be capable of observing near-field observations from the solar oscillations provided they are sufficiently large.

8.2 Solar Gravitational Perturbations

We start by attempting to derive the results of (Cutler & Lindblom, 1996) for perturbation in gravitational potential which could be detectable by gravitational wave detectors of the future. We start the analysis with the perturbation to newtonian potential

$$\Phi = \Phi_0 + \delta\Phi \tag{8.1}$$

we can use the poisson equation

$$\nabla^2\Phi = 4\pi G\rho \tag{8.2}$$

to separate the density in a similar way. Since we are interested in potential outside the sun, near earth orbit, we just need to solve

$$\nabla^2\Phi = 0 \tag{8.3}$$

Solving this well known problem in spherical polar coordinates:

$$\frac{1}{r^2}\frac{\partial}{\partial r}\left(r^2\frac{\partial\Phi}{\partial r}\right) + \frac{1}{r^2\sin\theta}\frac{\partial}{\partial\theta}\left(\sin\theta\frac{\partial\Phi}{\partial r}\right) + \frac{1}{r^2\sin^2\theta}\frac{\partial^2\Phi}{\partial\varphi^2} = 0 \tag{8.4}$$

We assume azimuthal symmetry, and then use variable separation as $\Phi(r,\theta) = \mathcal{R}(r)\Theta(\theta)$. Then,

$$\frac{1}{\mathcal{R}}\frac{d}{dr}\left(r^2\frac{d\mathcal{R}}{dr}\right) = -\frac{1}{\Theta\sin\theta}\frac{dl}{d\theta}\left(\sin\theta\frac{d\Theta}{d\theta}\right) = l(l+1) \tag{8.5}$$

where $l(l+1)$ is a dimensionless constant. Thus, the radial solution by inspection is

$$\mathcal{R}(r) = Ar^l + \frac{B}{r^{l+1}} \tag{8.6}$$

and the angular solution is just set of *Legendre polynomials*:

$$\Theta(\theta) = P_l(\cos\theta) \tag{8.7}$$

Then the solution in terms of all variables is

$$\Phi_l(r,\theta,\varphi,t) = \left(A_l' r^l + \frac{B_l'}{r^{l+1}}\right) P_l \cos\theta e^{im\varphi} e^{i\omega t} \tag{8.8}$$

where m, ω are constants. Since the equation (8.3) is linear in Φ, we get a full general solution as

$$\Phi(r,\theta,\varphi,t) = \sum_{l,m} \left(A_l r^l + \frac{B_l}{r^{l+1}}\right) \cdot Y_l^m(\theta,\varphi) e^{i\omega t} \tag{8.9}$$

where $Y_l^m(\theta,\varphi)$ are the spherical harmonics, which when written in terms of Legendre polynomials have some normalization constants which have been absorbed into A_l and B_l. Now, we need to invoke boundary conditions. Firstly, since $\Phi(r=\infty)=0$, all the constants $A_l = 0$. Next, the boundary condition for unperturbed potential at surface is just $\Phi_0(R) = -GM_\odot/R_\odot$, which corresponds to $B_0 = -GM$. Now define

$$B_l = \Phi_0 R_\odot^{l+1} \alpha_l \tag{8.10}$$

where α_l is a dimensionless proportionality constant depending on l ($\alpha_0 = 1$). Now, since the gravitational perturbation is directly caused by moving fluid, $\delta\Phi \propto$ perturbed fluid velocity. Thus, the helioseismic mode energy will vary as

$$E = \int \rho \delta v_a^* \delta v^a d^3x \tag{8.11}$$

where δv^a is the fluid velocity perturbation. Thus,

$$\delta\Phi_l \propto \sqrt{E} \tag{8.12}$$

which implies

$$\delta\Phi = \alpha_{28} \left(\frac{E}{10^{28}\text{ergs}}\right)^{1/2} \frac{GM_\odot}{R_\odot} \left(\frac{R_\odot}{r}\right)^{l+1} Y_{lm} e^{i\omega t} \tag{8.13}$$

where r is the distance from centre of sun, α_{28} (calculated numerically from a standard solar model) is the magnitude of external gravitational perturbation from an oscillation mode normalized to have energy $E = 10^{28}$ergs. Note that this equation considers only newtonian potentials.

The numerical calculation uses the equation of state of a normal solar model (model 1 of (Christensen-Dalsgaard et al., 1993)), and treats the pulsations as small amplitude perturbations following linear adiabatic evolution equations (Cutler & Lindblom, 1996).

Now, M_{mode} (mode mass) is defined as the ratio of mode energy E and the average surface velocity of the mode

$$E = \frac{M_{mode}}{4\pi} \int \delta v^a \delta v_a^* \sin\theta d\theta d\varphi \tag{8.14}$$

The mode masses help convert observable surface velocities of modes into mode energies. Only $l = 2$ modes have been considered since modes with higher l have their gravitational wave signals reduced by factors of $(R_\odot/r) \approx 0.005$.
The paper (Cutler & Lindblom, 1996) uses numerical analysis to find the largest gravitational perturbation - corresponding to $l = 2$ g_3 mode when modes excited to equal energy levels are compared. The surface is oversimplified in this treatment - using realistic equation of state for densities above $10^{-6}\, gm\, cm^{-3}$, while below these densities a smooth polytropic "atmosphere" is attached.
This results in errors of about 0.01% for ω and α_{28}, but higher errors upto 10% for M_{mode}.

8.3 Gravitational Waves

To study what are gravitational waves and their effects on the physical world, we start by analysing their origins through the general theory of relativity. Beginning with the einstein equations,

$$R_{\mu\nu} - \frac{1}{2} g_{\mu\nu} R = \frac{8\pi G}{c^4} T_{\mu\nu} \tag{8.15}$$

where $R_{\mu\nu}$ is the Ricci tensor, R is the Ricci Scalar and $T_{\mu\nu}$ is the energy-momentum tensor. The study of gravitational waves appreciably far from the source can be done by linearising the metric tensor as follows

$$g_{\mu\nu} = \eta_{\mu\nu} + h_{\mu\nu} \tag{8.16}$$

where $\eta = diag(1, -1, -1, -1)$ is the Minkowski metric and $h_{\mu\nu}$ is the deviation from flat spacetime. Consider the change in coordinates

$$x^\mu \to x'^\mu = x^\mu + \xi^\mu \tag{8.17}$$

where the derivatived $|\partial\xi^\mu|$ are at max of the same order as $|h_{\mu\nu}$. Then, the transformation of $h_{\mu\nu}$ to the lowest order will be

$$h_{\mu\nu}(x) \to h'_{\mu\nu}(x') = h_{\mu\nu}(x) - (\partial_\mu \xi_\nu + \partial_\nu \xi_\mu) \tag{8.18}$$

We observe that $h_{\mu\nu}$ is invariant under Poincare Transformations as long as the Lorentz boosts do not spoil the condition $|h_{\mu\nu}| \ll 1$.
To linear order in $h_{\mu\nu}$, the Riemann tensor becomes

$$R_{\mu\nu\rho\sigma} = \frac{1}{2}(\partial_\nu \partial_\rho h_{\mu\sigma} + \partial_\mu \partial_\sigma h_{\nu\rho} - \partial_\mu \partial_\rho h_{\nu\sigma} - \partial_\nu \partial_\sigma h_{\mu\rho}) \tag{8.19}$$

Now define the trace reversed metric by

$$\bar{h}_{\mu\nu} = h_{\mu\nu} - \frac{1}{2}\eta_{\mu\nu} h \tag{8.20}$$

where $h = \eta^{\mu\nu} h_{\mu\nu}$. Thus, solving the Einstein equations (8.15) using the above results, we arrive at

$$\Box \bar{h}_{\mu\nu} + \eta_{\mu\nu} \partial^\rho \partial^\sigma \bar{h}_{\rho\sigma} - \partial^\rho \partial_\nu \bar{h}_{\rho\mu} - \partial^\rho \partial_\mu \bar{h}_{\nu\rho} = -\frac{16\pi G}{c^4} T_{\mu\nu} \tag{8.21}$$

We can now use the Lorentz Gauge freedom of linearised gravity to choose

$$\partial^\nu \bar{h}_{\mu\nu} = 0 \tag{8.22}$$

to arrive at the simple wave equation

$$\Box \bar{h}_{\mu\nu} = -\frac{16\pi G}{c^4} T_{\mu\nu} \tag{8.23}$$

Upon further analysis and moving to the TT Gauge, we arrive at the result

$$m\ddot{\xi}^i = \frac{m}{2} \ddot{h}^i{}_j \xi^j \tag{8.24}$$

Thus, here we see

$$h \sim \frac{\ddot{\xi}_{change}}{\xi_{init}} \tag{8.25}$$

which means h represent a sort of strain in the coordinate shift

8.4 LISA

Since the solar oscillations of $l \geq 2$ have a non-zero quadrupole or order multipole moment, they will give rise to gravitational waves. The current state-of-the-art gravitational wave detectors are the two LIGO detectors located in USA. These have a strain sensitivity of upto $10^{-23}/\sqrt{\text{Hz}}$. However, they are most sensitive in the frequency region of $10 - 1000$ Hz, and are limited by seismic noise at the lower end of the frequency spectrum (Aasi et al., 2015). On the other hand, solar g-modes have much lower frequencies - of the order of 10^{-4} Hz for lower n, l values. Thus, they are not detectable by LIGO.

LISA is a mission proposed by ESA/NASA which will be a space based gravitational wave interferometric antenna. This mission will be sensitive to gravitational waves in the frequency range 10^{-4}Hz to 1 Hz. It will consist of three spacecraft at the vertices of an equilateral triangle of sides 5×10^9m. Current analyses through ground based testing, theory and the hugely successful LISA Pathfinder mission indicate towards an instrumental noise of $3 * 10^{-18}$/Hz at 10^{-4} Hz. Current estimates of confusion noise from binaries will be of a comparable order of magnitude. For one year of observation, dimensionless strain with SNR > 5 that is detectable would be of order $10^{-21} - 10^{-20}$ Additionally, LISA will also be sensitive to time-dependent variations in the gravitational field of the same frequency range. If the solar g-modes have large enough amplitudes, they could produce variations in the gravitational field at 1 a. u. which could be detectable by a LISA type interferometer. (Amaro-Seoane et al., 2017)

To see the effect of time dependent perturbations of the gravitational field from the sun on LISA, consider the geodesic equation

$$\frac{d^2x^\mu}{d\tau^2} + \Gamma^\mu_{\nu\rho}(x)\frac{dx^\nu}{d\tau}\frac{dx^\rho}{d\tau} = 0 \tag{8.26}$$

Now, for two nearby geodesics (being followed by the satellites of LISA), where one is parametrized by $x^\mu(\tau)$ and the other by $x^\mu(\tau) + \xi^\mu(\tau)$, then $x^\mu(\tau)$ will satisfy (8.26) while $x^\mu(\tau) + \xi^\mu(\tau)$ satisfies

$$\frac{d^2(x^\mu + \xi^\mu)}{d\tau^2} + \Gamma^\mu_{\nu\rho}(x+\xi)\frac{d(x^\nu + \xi^\nu)}{d\tau}\frac{d(x^\rho + \xi^\rho)}{d\tau} = 0 \tag{8.27}$$

If the perturbation $|\xi^\mu|$ is much smaller than typical scale of variation of gravitational field then subtracting the geodesic equations and keeping terms upto first order, we get

$$\frac{d^2\xi^\mu}{d\tau^2} + 2\Gamma^\mu_{\nu\rho}(x)\frac{dx^\nu}{d\tau}\frac{d\xi^\rho}{d\tau} + \xi^\sigma\partial_\sigma\Gamma^\mu_{\nu\rho}(x)\frac{dx^\nu}{d\tau}\frac{dx^\rho}{d\tau} = 0 \tag{8.28}$$

We can rewrite this in a more elegant form

$$\frac{D^2\xi^\mu}{D\tau^2} = -R^\mu{}_{\nu\rho\sigma}\xi^\rho\frac{dx^\nu}{d\tau}\frac{dx^\sigma}{d\tau} \tag{8.29}$$

where D represents the covariant derivative of a vector field $V^\mu(x)$ along the curve $x^\mu(\tau)$ and $R^\mu{}_{\nu\rho\sigma}$ is the Riemann curvature tensor. Since we have been working with the weak field approximation till now, we define the corresponding metric by

$$ds^2 = g_{\mu\nu}dx^\mu dx^\nu = (\eta_{\mu\nu} + h_{\mu\nu})dx^\mu dx^n u = -\left(1 + \frac{2\phi}{c^2}\right)dt^2 + \left(1 - \frac{2\phi}{c^2}\right)(dx^2 + dy^2 + dz^2) \tag{8.30}$$

where ϕ is approximately GM/r, $\eta = diag(1,-1,-1,-1)$ is the Minkowski metric and h is the perturbation due to sun's gravity. Then, to solve (8.29), we first use the slow motion approximation to get

$$\frac{d^2\delta l^\mu}{dt^2} = R^\mu{}_{0\rho0}l^\rho \tag{8.31}$$

In the weak field approximation, the required Riemann tensor will be

$$R^\mu{}_{0\rho0} = \Gamma^\mu_{0\rho,0} - \Gamma^\mu_{00,\rho} + \Gamma^\mu_{0\lambda}\Gamma^\lambda_{0\rho} - \Gamma^\mu_{\rho\kappa}\Gamma^\kappa_{00} \approx \frac{1}{2}\eta^{\mu\nu}(h_{\rho\nu,00} - h_{0\nu,0\rho} + h_{00,\nu\rho} + h_{0\rho,\nu0}) \tag{8.32}$$

From the equation above, $R^0{}_{0\rho0} = 0$ which when used in (8.31) gives $d^2\delta l^0/dt^2 = 0$.
Thus, from $h_{0i} = 0$, $l^\alpha = l^\alpha_0 + \delta l^\alpha$

$$\frac{d^2\delta l^i}{dt^2} = \frac{1}{2}\left[\eta^{ik}\frac{d^2h_{kj}}{dt^2} - c^2\eta^{im}\nabla_m\nabla_j h_{00}\right]l^j_0 \tag{8.33}$$

where roman indices i, j, k, m etc represent spatial coordinate indices. For constant frequency gravitational waves causing the change in length between LISA's arms, we write

$d^2\delta l/dt^2 = \omega^2\delta l$. Also, for gravitational waves we only consider the perturbed potential in h, giving us

$$\omega^2\delta L = L\, n^a n^b \nabla_a \nabla_b \delta\Phi \tag{8.34}$$

where L is the mean distance between satellites, n^a is a unit vector in the direction of line of satellites Defining the dimensionless strain h that would be measured by a detector consisting of two perpendicular interferometer arms:

$$h = \omega^{-2}(n^a n^b - m^a m^b)\nabla_a \nabla_b \delta\Phi \tag{8.35}$$

where n^a and m^a are unit vector arms pointing in the directions of the two detector arms. The RHS depends on orientation of plane of detector arms, the orientation of the arms in this plane, the position of centre of mass of the satellites, and the l and m of the mode. Using the average value for this quantity - first taking average over all orientations of the 2 arms at a fixed point in space:

$$< |(n^a n^b - m^a m^b)\nabla_a \nabla_b \delta\Phi|^2 >= \frac{2}{5}\nabla_a \nabla_b \delta\Phi \nabla^a \nabla^b \delta\Phi^* \tag{8.36}$$

Now averaging over all possible locations of the satellite around the sun

$$< |h|^2 >= \frac{1}{10\pi}\int \nabla_a \nabla_b \delta\Phi \nabla^a \nabla^b \delta\Phi^* \sin\theta d\theta d\Phi \tag{8.37}$$

Using the expression for $\delta\Phi$, we get the average strain h:

$$h = \alpha_{28}\sqrt{(l+1)(l+2)(2l+1)(2l+3)} \times \left(\frac{1}{10\pi}\right)^{1/2}\left(\frac{E}{10^{28}\text{ ergs}}\right)^{1/2}\frac{GM_\odot}{\omega^2 R_\odot^3}\left(\frac{R_\odot}{r}\right)^{l+3} \tag{8.38}$$

Modes of same n and l but different m have frequencies that are slightly split by the sun's rotation. Over a year LISA will be able to distinguish frequencies within $\Delta f \approx 3\times 10^{-2}\mu$Hz (for SNR ~ 1). This is roughly an order of magnitude smaller than the size of splitting due to sun's rotation, and thus modes with different m are effectively non degenerate.

8.5 Signal Strengths and Noise Levels

- Since the modes that can be observed by LISA have not been observed to date, making reliable predictions of the energy contained in these modes difficult. The observed low l p-modes have a maximum energy/mode of roughly 10^{28} ergs for f near 3000 μHz, which decreases to 10^{27} ergs for f near 1000 μHz.
- At low frequencies, the detection by doppler shifts becomes difficult due to decrease in surface velocity (decreasing as $f^{3.5}$ for p-modes and f^2 for g modes) but increase in instrumental and background surface velocity noise. The observational upper limit on surface velocities for these is about 4 $cm\ s^{-1}$, as stated in Cutler & Lindblom (1996). Note that these limits have subsequently been tightened through direct analysis of combined data from multiple sources, or through indirect means. The implications of the new limits will be covered in later sections. The old observational limits correspond

TABLES

TABLE I. Gravitational Parameters of Solar Oscillations.

Mode	f (μHz)	α_{28}	$M_{\rm mode}$ (gm)	h	$E_{\rm min}$(erg)	$E_{\rm max}$(erg)
g_3	220.4	7.17×10^{-12}	8.3×10^{31}	1.18×10^{-23}	1.55×10^{30}	1.3×10^{33}
g_2	254.0	6.07×10^{-12}	4.4×10^{31}	7.50×10^{-24}	1.97×10^{30}	7.0×10^{32}
p_1	381.6	5.31×10^{-12}	4.3×10^{30}	2.91×10^{-24}	2.02×10^{30}	6.9×10^{31}
g_4	192.2	5.96×10^{-12}	1.9×10^{32}	1.29×10^{-23}	2.42×10^{30}	3.0×10^{33}
g_5	168.8	4.72×10^{-12}	3.5×10^{32}	1.32×10^{-23}	4.19×10^{30}	5.6×10^{33}
g_1	293.6	2.81×10^{-12}	2.3×10^{31}	2.60×10^{-24}	8.44×10^{30}	3.7×10^{32}
f	350.9	2.31×10^{-12}	1.2×10^{31}	1.50×10^{-24}	1.12×10^{31}	1.9×10^{32}
p_2	514.4	2.02×10^{-12}	5.5×10^{29}	6.07×10^{-25}	1.17×10^{31}	8.8×10^{30}
g_6	134.0	2.80×10^{-12}	8.2×10^{32}	1.24×10^{-23}	1.37×10^{31}	1.3×10^{34}
p_3	663.6	8.60×10^{-13}	1.4×10^{29}	1.56×10^{-25}	5.53×10^{31}	2.2×10^{30}
g_7	101.2	1.42×10^{-12}	1.6×10^{33}	1.10×10^{-23}	6.30×10^{31}	2.6×10^{34}

Figure 15: The heliosesimic modes of different n values are listed for $l = 2$. The frequencies are functions of n, l values, along with other observables and thus do not assume any particular solar model. The α_{28} and M_{mode} values are calculated using a standard solar model model 1 of 1993 paper). h is the gravitational strain calculated from (8.38) using $E = 10^{28} ergs$. E_{min} is the minimum energy required by the modes to have an SNR of 3 in LISA, and E_{max} is the upper constraint on the modes obtained from observations of solar surface velocities and using the mode mass in the table (Cutler & Lindblom, 1996).

to the max mode energies in Table 1. The paper by Christensen-Dalsgaard et al. (1993) suggests that the low SNR 'detections' of solar g modes are an indication that the g mode energies are right under the current maximum values. This would be easily detectable by LISA.

- The paper by Kumar et al. (1995) have made predictions of energies of low frequency g-modes by considering a turbulent convection excitation mechanism (Goldreich et al., 1994). This predicts an average energy of 10^{28} ergs, if the dissipation time of the modes is assumed to be 10^6 years.
- For frequencies below 1000μHz, LISA will be able to detect signals above the amplitudes

$$h_{sp} = 3 \times 10^{-22} \left(\frac{f}{100 \mu \text{Hz}} \right)^{-2.3} \tag{8.39}$$

due to noise.

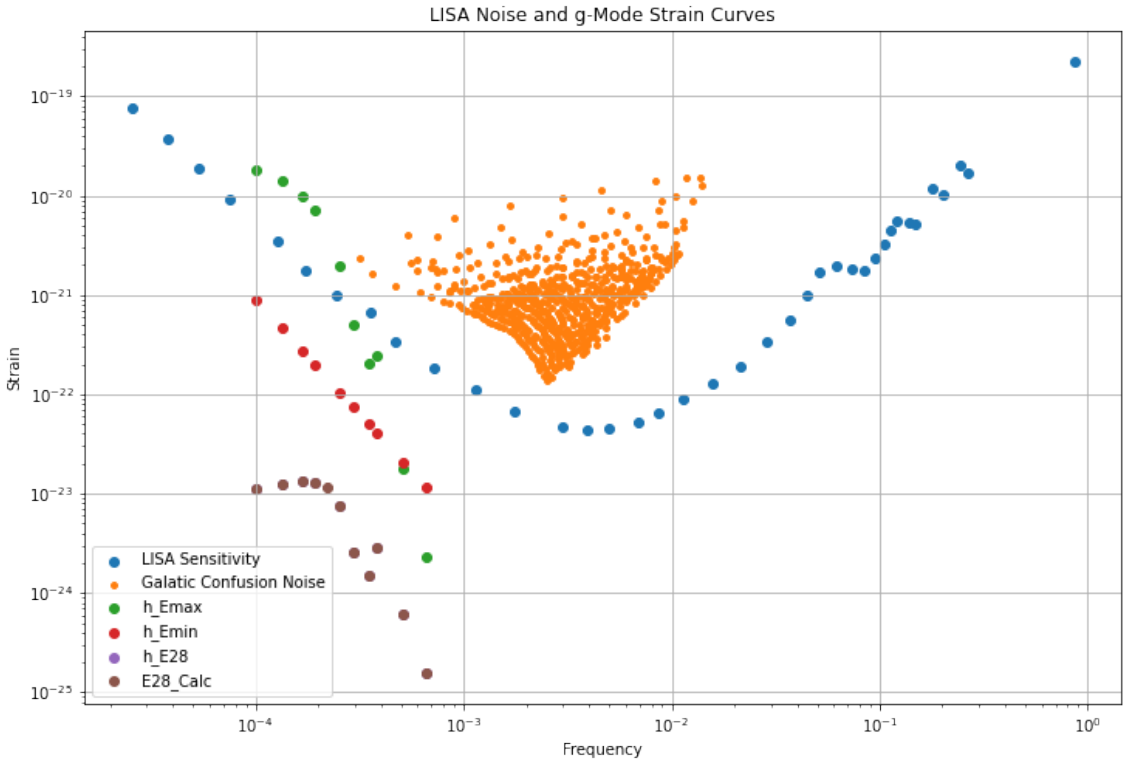

Figure 16: This is a figure of the dimensionless strain plotted against frequency in logarithmic scale, with the strain values for g-modes of energies of 10^{28}, E_{min} and E_{max} from the table (15). Along with it, LISA's projected sensitivity from the L3 proposal is plotted (Amaro-Seoane et al., 2017), along with a rough representation of the region of Galactic Binary Confusion Noise (Nelemans et al., 2001).

As we see from the plot 16, the solar g-mode sensitivity would have to be close to the maximum allowed value from current observation limits for it to be detectable by a LISA type detector. Moreover, we can conclude that a better analysis of the gravitational waves produced by g-modes can be helpful, where we can include effects of relativistic treatment of gravitational potentials and updated models of the solar surface.

8.6 Discussion

- The paper uses approximations for the production of gravitational waves from g-modes, which can be imporved upon
- The effect of a stochastic background of gravitational waves would have to be looked at with more care, since it has an appreciable amplitude at frequencies of interest
- The sensitivity levels used in this analysis tells that unless g-modes have the highest allowed energies according to current observational limits on solar surface velocities, LISA will not be able to detect the g-modes with appreciable SNR. Thus, a closer analysis is called for.

9 Quadrupole Moment Analysis of Solar g modes

9.1 Solar Oscillations and Metric Perturbation Field Around the Sun

Solar oscillations can be modelled in the way of the paper (Polnarev et al., 2009) by considering a surface harmonic with any variable, such as radial displacement δr, as:

$$\frac{\delta r(\mathbf{r},t)}{R_\odot} = \sum_{l=0}^{\infty}\sum_{m=-l}^{l}\sum_{n=-\infty}^{\infty} \zeta_{nlm}(r) S_{lm}(\theta\phi) e^{i\omega t} \tag{9.1}$$

Here ζ_{nlm} are dimensionless eigenfunctions, S_{lm} are the spherical harmonics and ω is the frequency of any particular mode. Due to sun's rotation, the degeneracy about the azimuthal mode m is lifted as $\omega_{nlm} \approx \omega_{nl0} + m\bar{\Omega}$, where $\bar{\Omega}$ is the weighted mean solar angular velocity $\sim 3 \times 10^{-6}$ rad/sec.
We also note that we only consider oscillations of $l = 2$, since external gravitational potential of a multipole of order l decreases as r^{l+1}, as seen in 8.13.
External newtonian grav potential can then be written as:

$$U(\mathbf{r},t) = -G\int_\odot \frac{\rho dV}{r} = U_0(\mathbf{r}) - \frac{G}{6}\mathcal{D}^{\alpha\beta}\nabla_{\alpha\beta}\left(\frac{1}{r}\right) = U_0(\mathbf{r}) - GM_\odot R_\odot^2 \sum_{m=-2}^{2}\sum_{n=-\infty}^{\infty} \frac{J_{nm}}{r^3} S_{2m}(\theta\phi) \tag{9.2}$$

where $U_0(\mathbf{r})$ is the time independent potential, $J_{nm} \propto e^{i\omega}t$ is the dimensionless time dependent quadrupole moments corresponding to eigenmodes with cyclical frequencies $\omega = \omega_{n2m}$.
In the above expression, $\mathcal{D}^{\alpha\beta}$ is given by

$$\mathcal{D}^{\alpha\beta} = \int_\odot \left(3x^\alpha x^\beta - \delta^{\alpha\beta}x^\mu x_\mu\right)\rho(t)dV = M_\odot R_\odot^2 \sum_{n=-\infty}^{\infty}\sum_{m=-2}^{2} C_m J_{nm}\mathcal{I}_m^{\alpha\beta} \tag{9.3}$$

Note that we are now using the convention where greek indices α, β represent the cartesian coordinates only. In the above equation, $C_0 = -\sqrt{5/4\pi}, C_m = \sqrt{15/4\pi}$ (for $m \neq 0$).

9.2 Quadrupole Moment of Helioseismic Modes

One way to evaluate the quadrupole moment $\mathcal{D}^{\alpha\beta}$ is to start from first principles by considering a simplified model of the Sun, with an observer at $\mathbf{r}$, as shown in figure 17. Consider the gravitational potential at $\mathbf{r}$ due to volume element at $\mathbf{r}'$:

$$U(\mathbf{r},t) = -G\int_\odot \frac{dm}{\mid \mathbf{r} - \mathbf{r}' \mid} \tag{9.4}$$

where $dm = dr'^3\rho(\mathbf{r}',t)$

$$U(\mathbf{r},t) = -G\int_\odot \frac{dr'^3}{\mid \mathbf{r} - \mathbf{r}' \mid}\rho(\mathbf{r}',t) \tag{9.5}$$

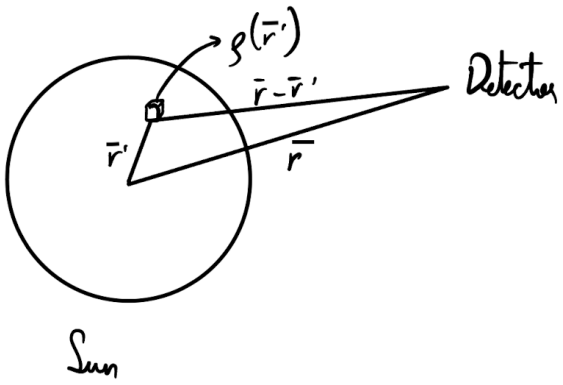

Figure 17: We consider a volume element dr'^3 in the sun denoted by position vector $\mathbf{r}'$ and an observer located at $\mathbf{r}$. The density at $\mathbf{r}'$ at time t is given by $\rho(\mathbf{r}', t)$

Here, use the first order approximation for density as

$$\rho(\mathbf{r}', t) = \rho_0(\mathbf{r}') + \delta\rho(\mathbf{r}', t) \tag{9.6}$$

Now, we expand the variation in density as a harmonic series as follows:

$$\frac{\delta\rho(\mathbf{r}', t)}{\rho_0(\mathbf{r}')} = \sum_{l,m} c_{lm} Y_m^l(\theta', \varphi') \Phi_{lm}(\mathbf{r}', t) \tag{9.7}$$

where c_{lm} are the coefficients of expansion for the harmonic series, Y_m^l are the spherical harmonics and $\Phi_{lm}(\mathbf{r}', t)$ is a perturbation term due to the lmth helioseismic mode. The coefficients c_{lm} will depend on the nature of perturbations and can be found by orthogonality of harmonics. Thus,

$$\delta\rho(\mathbf{r}', t) = \rho_0(\mathbf{r}') \sum_{l,m} c_{lm} Y_m^l(\theta', \varphi') \Phi_{lm}(\mathbf{r}', t) \tag{9.8}$$

Now consider the quadrupole moment as defined in 9.3,

$$\mathcal{D}^{\alpha\beta} = \int_\odot (3r'^\alpha r'^\beta - \delta^{\alpha\beta} r'^2) \delta\rho(\mathbf{r}', t) d^3r \tag{9.9}$$

$$= \sum_{l,m} \int_\odot (3r'^\alpha r'^\beta - \delta^{\alpha\beta} r'^2) \rho_0(\mathbf{r}') c_{lm} Y_m^l(\theta', \varphi') \Phi_{lm}(\mathbf{r}', t) d^3r \tag{9.10}$$

where $\alpha, \beta \in \{1, 2, 3\}$ and r'^α is given as

$$r'^1 = r' \sin\theta' \cos\varphi' \tag{9.11}$$

$$r'^2 = r' \sin\theta' \sin\varphi' \tag{9.12}$$

$$r'^3 = r' \cos\theta' \tag{9.13}$$

Now separate the Φ_{lm} perturbation term into radial amplitude and frequency terms as

$$\Phi_{lm}(\mathbf{r}', t) = \sum_n e^{\iota\omega_{nlm} t} \xi(\mathbf{r}') h_{nlm} \tag{9.14}$$

where ω_{nlm} is the frequency of modes, $\xi(\mathbf{r}')$ represents the normalized eigenmodes and h_{nlm} is the amplitude of nlm^{th} mode.
Note that $\mathcal{D}^{\alpha\beta}$ is a 3×3 traceless matrix, and that the quadrupole term has relevant contributions for $l = 2$ only.
Now expand the integral in 9.9 as

$$\mathcal{D}^{\alpha\beta} = \sum_{n,m} e^{\iota\omega_{n2m}t} h_{n2m} \tag{9.15}$$

$$\times \int_0^{R_\odot} r'^2 dr' \rho_0(\mathbf{r}') \xi(\mathbf{r}') r'^2 \tag{9.16}$$

$$\times \int_0^{2\pi} \int_0^{\pi} \frac{(3r'^\alpha r'^\beta - \delta^{\alpha\beta} r'^2)}{r'^2} Y_m^2(\theta', \varphi') \sin\theta' d\theta' d\varphi' \tag{9.17}$$

Rearranging,

$$\mathcal{D}^{\alpha\beta} = \sum_{n,m} e^{\iota\omega_{n2m}t} h_{n2m} M_\odot R_\odot^2 \tag{9.18}$$

$$\times \int_0^{R_\odot} \frac{r'^2 dr' \rho_0(\mathbf{r}')}{M_\odot} \xi(\mathbf{r}') \frac{r'^2}{R_\odot^2} \tag{9.19}$$

$$\times \int_0^{2\pi} \int_0^{\pi} \frac{(3r'^\alpha r'^\beta - \delta^{\alpha\beta} r'^2)}{r'^2} Y_m^2(\theta', \varphi') \sin\theta' d\theta' d\varphi' \tag{9.20}$$

Comparing to 9.3, we can write

$$J_{nm} = \left[\int \frac{r'^2 dr' \rho_0(\mathbf{r}')}{M_\odot} \xi(\mathbf{r}') \frac{r'^2}{R_\odot^2} \right] h_{n2m} \tag{9.21}$$

where the part in [ ] might be an $\mathcal{O}(1)$ number.
The integral of the angular parts in 9.18 have been displayed in table 18. Note that in the expression of 9.18, we have a few unknowns - namely $\omega_{n2m}, h_{n2m}, \rho_0(\mathbf{r}')$ and $\xi(\mathbf{r}')$. These are usually obtained through a combination of simulations of the Sun, or are bounded by current limits on observables.
We have been working on simulating the solar interior using ADIPLS (**?**) - a code that numerically simulates the interior of the sun by considering various parameters which can be modified by the user. This can allow us to find the profiles of various parameters such as density, sound speed profile etc. and simulate helioseismic oscillations. By simulating the oscillations we will be able to obtain eigenfunctions and eigenfrequencies for the modes, as required.
Finally, the codes will not give accurate results on h_{n2m}, so we can evaulate the results by using some expected values, and by considering the observational upper bounds. The latter can be done by various methods such as converting observational limits on solar surface velocities across various surveys, or through g mode amplitude estimates through indirect measurements of g-modes in mixed modes.

Consider the solar surface velocities $\mathbf{v}$ through the continuity equation

$$\frac{\partial \rho}{\partial t} + \nabla \cdot (\rho \mathbf{v}) = 0 \tag{9.22}$$

m	D^{11}	D^{12}	D^{13}	D^{22}	D^{23}	D^{33}
-2	$\sqrt{\frac{15}{16\pi}\frac{8\pi}{5}}$	$\sqrt{\frac{15}{16\pi}\frac{8\pi}{5}}$	0	0	0	0
-1	0	0	0	0	$\sqrt{\frac{15}{16\pi}\frac{8\pi}{5}}$	0
0	$-\sqrt{\frac{5}{16\pi}\frac{8\pi}{5}}$	0	0	$-\sqrt{\frac{5}{16\pi}\frac{8\pi}{5}}$	0	$\sqrt{\frac{5}{16\pi}\frac{16\pi}{5}}$
1	0	0	$\sqrt{\frac{15}{16\pi}\frac{8\pi}{5}}$	0	0	0
2	0	0	0	$-\sqrt{\frac{15}{16\pi}\frac{8\pi}{5}}$	0	0

Figure 18: The angular parts of the integral are listed here. $\mathcal{D}^{\alpha\beta}$ is symmetric, so it would have 6 independent terms. However, since we are summing over m, we get 30 independent terms, many of which vanish.

Considering the first order expansion of density as in 9.6, then we can expand the continuity equation as

$$\frac{\partial(\delta\rho)}{\partial t} + \nabla \cdot (\rho_0 \mathbf{v}) = 0 \tag{9.23}$$

Note that under the assumption that the star is static, $\mathbf{v}$ should be a first order term itself, and thus we can ignore the higher order term of $\rho_1 \mathbf{v}$. Thus,

$$\frac{\partial(\delta\rho)}{\partial t} + \rho_0(\nabla \cdot \mathbf{v}) + \mathbf{v} \cdot (\nabla\rho_0) = 0 \tag{9.24}$$

Now, if we invoke spherical symmetry, the tangential derivatives of equilibrium quantities will vanish. Thus,

$$\frac{\partial(\delta\rho)}{\partial t} + \rho_0(v_{r,r} + v_{t,t}) + v_r\rho_{0,r} = 0 \tag{9.25}$$

where subscripts after comma denote derivative with respect to that component. Here r denotes radial components and t denotes tangential components. We can now evaluate these terms through the density profile from the code, and by considering the velocity functions as

$$v = v_0 e^{\iota\omega_{n2m}t}\xi'(\mathbf{r}') \tag{9.26}$$

where the eigenfunctions $\xi'(\mathbf{r}')$ can be evaluated by code, and the amplitudes can be provided by observational limits. A diagram showing the observational limits through a survey of various solar observatories is shown in figure 19.

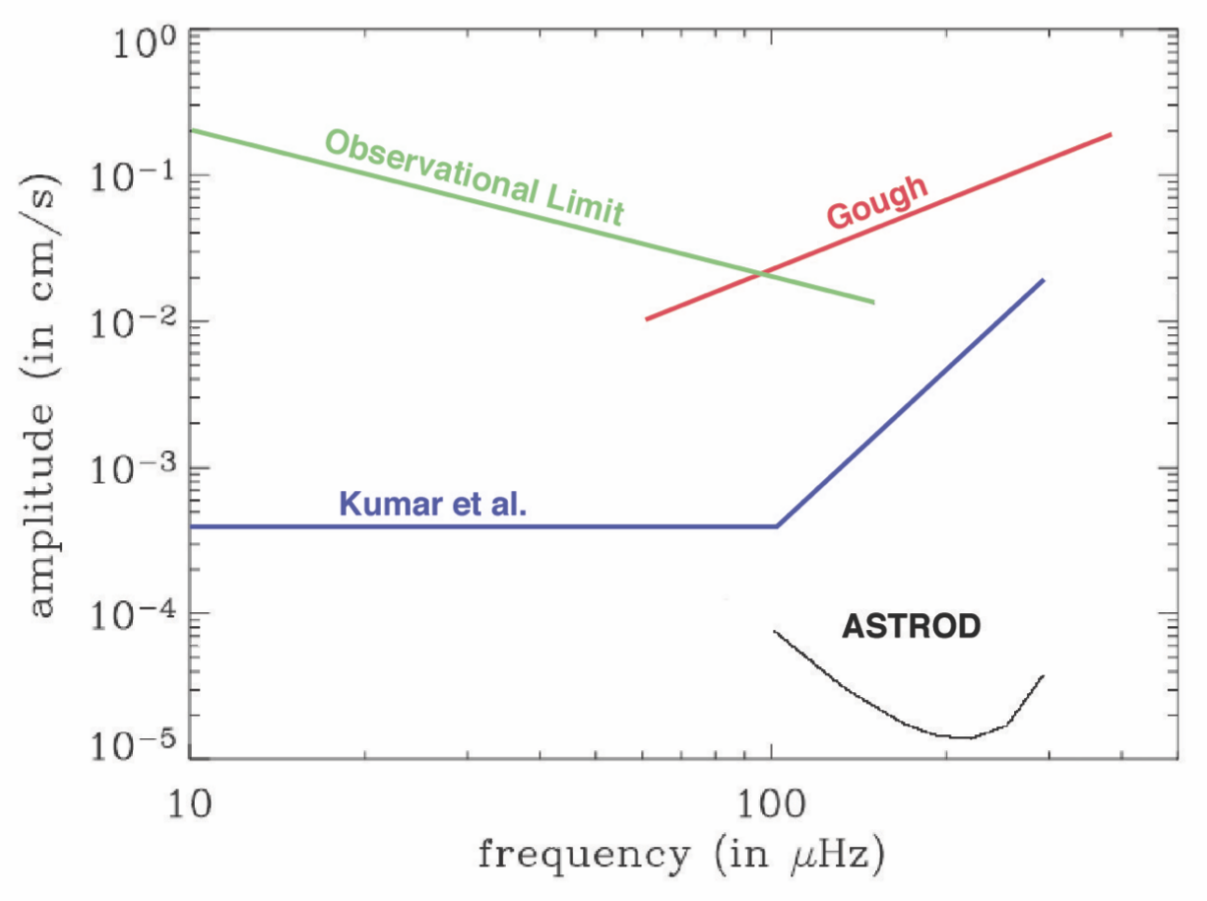

Figure 19: The observational limits in this paper are obtained by the survey of the Michelson Doppler Interferometer (MDI) and Variability of solar IRradiance and Gravity Oscillations (VIRGO) aboard the Solar and Helioseismic Observatory (SOHO) spacecraft, as well as ground based observations by Birmingham Solar Oscillations Network (BiSON) and Global Oscillations Network Group (GONG). (Appourchaux et al., 2000) (Burston et al., 2008)

9.3 Conclusions

- Once the frequencies, eigenfunctions and density profiles are evaluated using the simulations, we will be able to evaluate the quadrupole moments of various g modes for a given amplitude.
- We can use the current observational limits and use other estimates of amplitudes to simulate the signal to noise ratio at the proposed sensitivity curve for LISA

References

Aasi, J., et al. 2015, Class. Quant. Grav., 32, 074001, doi: 10.1088/0264-9381/32/7/074001

Agostini, M., Altenmüller, K., Appel, S., et al. 2020, The European Physical Journal C, 80, 1

Amaro-Seoane, P., Audley, H., Babak, S., et al. 2017, arXiv preprint arXiv:1702.00786

Appourchaux, T., Fröhlich, C., Andersen, B., et al. 2000, The Astrophysical Journal, 538, 401

Asplund, M., Grevesse, N., Sauval, A. J., & Scott, P. 2009, arXiv preprint arXiv:0909.0948

Basu, S. 2016, Living Reviews in Solar Physics, 13, 1

Basu, S., & Antia, H. 2008, Physics Reports, 457, 217

Basu, S., & Chaplin, W. J. 2017, Asteroseismic data analysis: foundations and techniques, Vol. 4 (Princeton University Press)

Bergemann, M., & Serenelli, A. 2014, in Determination of atmospheric parameters of B-, A-, F-and G-type stars (Springer), 245–258

Burston, R., Gizon, L., Appourchaux, T., Ni, W., et al. 2008in , IOP Publishing, 012043

Carroll, B. W., & Ostlie, D. A. 2017, An introduction to modern astrophysics (Cambridge University Press)

Cerdeno, D. G., Davis, J. H., Fairbairn, M., & Vincent, A. C. 2018, Journal of Cosmology and Astroparticle Physics, 2018, 037

Christensen-Dalsgaard, J., Di Mauro, M. P., Houdek, G., & Pijpers, F. 2009, Astronomy & Astrophysics, 494, 205

Christensen-Dalsgaard, J., Proffitt, C., & Thompson, M. 1993, The Astrophysical Journal, 403, L75

Chung, M. K., Dalton, K. M., & Davidson, R. J. 2008, IEEE transactions on medical imaging, 27, 1143

Cutler, C., & Lindblom, L. 1996, Physical Review D, 54, 1287

Fossat, E., Boumier, P., Corbard, T., et al. 2017, Astronomy & Astrophysics, 604, A40

Goldreich, P., Murray, N., & Kumar, P. 1994, Astrophysical Journal, 424, 466

Gough, D. 2019, Monthly Notices of the Royal Astronomical Society: Letters, 485, L114

Grevesse, N., & Sauval, A. 1998, Space Science Reviews, 85, 161

Kumar, P., Ao, C. O., & Quataert, E. J. 1995, arXiv preprint astro-ph/9503053

Maggiore, M. 2007, Gravitational waves: Volume 1: Theory and experiments (OUP Oxford)

Nelemans, G., Yungelson, L., & Zwart, S. P. 2001, Astronomy & Astrophysics, 375, 890

Pallé, P. L. 1991, Advances in Space Research, 11, 29

Polnarev, A., Roxburgh, I. W., & Baskaran, D. 2009, Physical Review D, 79, 082001

Sokolov, A. V. 2020, Journal of Cosmology and Astroparticle Physics, 2020, 013

Song, N., Gonzalez-Garcia, M. C., Villante, F. L., Vinyoles, N., & Serenelli, A. 2018, Monthly Notices of the Royal Astronomical Society, 477, 1397

Thomson, D. J., Maclennan, C. G., & Lanzerotti, L. J. 1995, Nature, 376, 139

Vagnozzi, S., Freese, K., & Zurbuchen, T. H. 2017, The Astrophysical Journal, 839, 55

Villante, F. 2010a, The Astrophysical Journal, 724, 98

—. 2010b, arXiv preprint arXiv:1001.2510

Vincent, A. C., Scott, P., & Serenelli, A. 2015a, Physical Review Letters, 114, 081302

Vincent, A. C., Serenelli, A., & Scott, P. 2015b, Journal of Cosmology and Astroparticle Physics, 2015, 040